(0.05%)–ethylenediaminetetraacetic acid (0.53 mmol/L) solution, collected by centrifugation, and cultured on plastic culture dishes containing standard medium until confluent. The cells were then trypsinized at 1:3 split ratio. Experiments were carried out with cells from the fourth to fifth passages. In this study, we established 3 primary cell isolations from different volunteers, and all cell isolations were used in each experiment. All 3 primary cell isolations were examined for the several extracellular matrix proteins by using reverse transcription–polymerase chain reaction. We confirmed that the cells expressed mRNA of type I collagen, dentin matrix protein-1 (DMP-1), and dentin sialoprotein; the latter 2 proteins are known to be specific to dentin (23). All primary cell isolations provided similar results in each experiment of this study.

Proliferation Assay

HDPC (6×10^4 cells/well) were plated onto 24-well plates until confluence. The cells were made quiescent by replacing the medium with serum-free α-MEM for 24 hours, and the medium was replaced with or without 1% FCS α-modified MEM in the presence or absence of FGF-2 (10 ng/mL). In another experiment mitomycin C (MMC) (Kyowa Hakko Kogyo Co, Tokyo, Japan) treatment was carried out before FGF-2 stimulation to suppress cell proliferation. Proliferation was assayed by pulsing wells with 185 kBq/w of [^{3}H]-thymidine (ICN Radiochemicals; Irvine, CA) during the last 4 hours of the culture. At the end of the incubation, cultures were harvested by using a semiautomatic cell harvester (Labomash; LM101 Laboscience, Tokyo, Japan), and [^{3}H]-thymidine incorporation was measured in a liquid scintillation counter (Aloka Co Ltd, Tokyo, Japan).

Alkaline Phosphatase Activity Assay

Alkaline phosphatase (ALPase) activity was investigated according to the procedure of Bessay et al (24). The HDPC were seeded in 24-well culture dishes (6×10^4 cells/well) with standard medium containing 50 μg/mL ascorbic acid and 10 mmol/L beta-glycerophosphate (BGP) (Sigma, St Louis, MO). Cells were cultured for the number of indicated days in this medium, and medium was changed every 3 days. We investigated ALPase activity when the HDPC were incubated with 10 ng/mL FGF-2 for 8, 14, 20, or 26 days. To determine the reversibility of the FGF-2 effect on ALPase activity, the HDPC were cultured for 15 days in the presence of FGF-2. Cells were then subsequently cultured in the absence of FGF-2 in standard medium containing 50 μg/mL ascorbic acid and 10 mmol/L BGP. After washing twice with saline, the cells were homogenized in a glass homogenizer in 1 mL of 0.9% NaCl, 0.2% Triton X-100 at 0°C–4°C, and centrifuged for 15 minutes at 12,000*g*. ALPase activity in the supernatant was measured by using *p*-nitrophenyl phosphate (*p*NP) as substrate. The supernatant was assayed in a 0.5 mol/L Tris/HCl buffer (pH 9.0) containing 0.5 mmol/L *p*NP and 0.5 mmol/L $MgCl_2$. The reaction mixture was incubated at 37°C for 30 minutes and was stopped by addition of 0.25 volume of 1 N NaOH. Hydrolysis of *p*NP was monitored as change in A410 with a spectrometer (Hitachi, Tokyo, Japan). *p*-Nitrophenol was used as a standard. One unit of activity was defined as the amount hydrolyzing 1 nmol of *p*-NP in 30 minutes.

Cellular DNA Content

DNA content was measured by a modification of the method of Labarca and Paigen (25). The HDPC were seeded in 24-well culture dishes (6×10^4 cells/well) with standard medium containing 50 μg/mL ascorbic acid and 10 mmol/L BGP. They were cultured for the indicated days with this medium, which was changed every 3 days. Alteration of DNA content of the cells was determined as follows. The HDPC were washed with phosphate-buffered saline and then homogenized at 0°C–4°C in 1 mL of 2 mol/L NaCl/25 mmol/L Tris-HCl (pH 7.4). After centrifugation at 12,000*g* for 10 minutes, 25 μL of 5 μg/mL bisbenzimidazole (Sigma) was added to 100 μL of the supernatant. The fluorescent spectra at emission (458 nm) after excitation at 356 nm were monitored by a spectrophotometer. The concentration of DNA in the samples was determined by a standard curve made at various concentrations of calf thymus DNA.

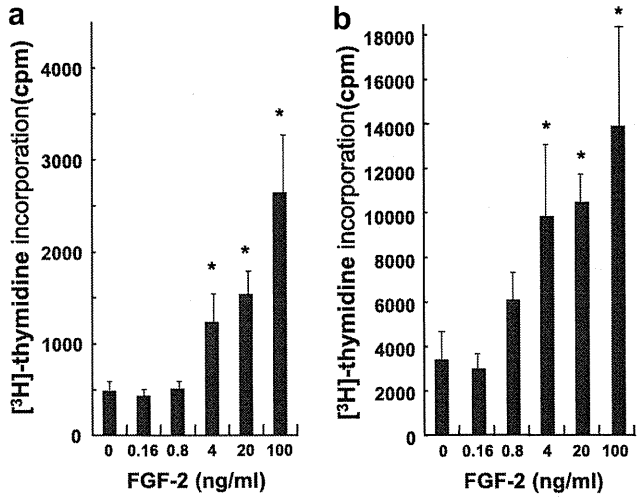

Figure 1. FGF-2 activates cell proliferation by HDPC. HDPC were incubated in 24-well plates until confluence. HDPC were made quiescent by replacing standard medium with serum-free alpha-MEM for 24 hours and cultured in the presence or absence of FGF-2 (0.16, 0.84, 4, 20, 100 ng/mL) without (*a*) or with (*b*) 1% FCS. Cells were pulsed with 185 kBq/w of [^{3}H]-thymidine during the last 4 hours of culture. At the end of the incubation, cultures were harvested, and the radioactivity was measured. Results of mean and standard error of the mean (SEM) of 3 identical experiments are shown. *$P < .05$.

Alizarin Red Staining

Cytochemical staining of calcium was performed by modification of the alizarin red staining method (26). HDPC were cultured on 6-well culture plates (4×10^5 cells/well). At the end of incubation with standard medium containing 50 μg/mL ascorbic acid and 10 mmol/L BGP for indicated time, cell layers were washed twice with saline and then fixed with dehydrated ethanol. After fixation, the cell layers were stained with 1% alizarin red S in 0.1% NH_4OH (pH 6.5) for 5 minutes and then washed with H_2O. Cells were observed under a microscope, and images were taken with a Nikon Coolpix (Nikon, Tokyo, Japan). Quantitative evaluation was determined by using image analysis with the WinRoof software program (Mitani Corporation, Fukui, Japan).

Migration Assay

Migration assays were performed after modifying the Teflon restraint migration assay (27). HDPC were seeded at 6×10^4 cells/glass bottom dish (Matsunami, Osaka, Japan), on which was placed a silicon block (30 mm × 70 mm; Togawa Rubber Co Ltd, Osaka, Japan) to introduce a cell-free area. Cells were grown until confluence, after which the silicon block was removed and the medium was replaced with 1% FCS α-MEM in the presence or absence of FGF-2 (10 ng/mL). The migration of HDPC to the cleared area was photographed immediately after removing the silicon block and 24 hours later by using a Nikon Eclipse TS100 inverted phase contrast microscope and Coolpix 990 (Nikon Corp). In each dish, 4 randomly chosen fields 1 mm in length were analyzed, and the number of cells that had translocated

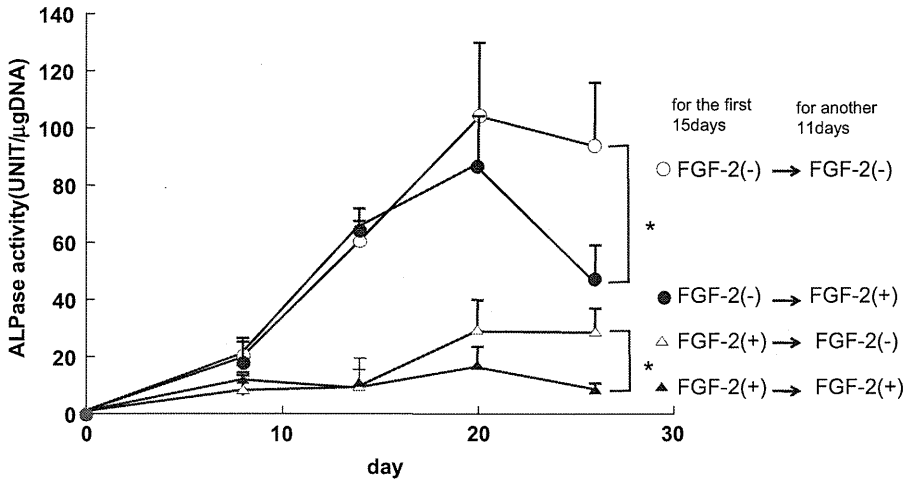

Figure 2. FGF-2 reversibly decreased ALPase activity by HDPC. HDPC were cultured with standard medium containing 50 μg/mL ascorbic acid and 10 mmol/L BGP in the presence or absence of FGF-2 (10 ng/mL). The 2 groups were then further subdivided, with the former cultures maintained in the continuous presence of FGF-2 (closed triangle) or FGF-2 was removed after 15 days, after which the culture continued to be incubated in the absence of FGF-2 (open triangle). The latter cultures were maintained in the absence of FGF-2 (open circle) or cultured with FGF-2 (closed circle). At the end of incubation, an ALPase assay was performed. Results of mean and SEM of 3 identical experiments are shown. *$P < .05$.

into the cleared area was determined. In some experiments HDPC were treated with 16 μg/mL of MMC for 2 hours at 37°C.

Statistical Analyses

All experiments were performed in triplicate, and results are expressed as mean ± standard deviation. Data were statistically analyzed between FGF-2–stimulated and unstimulated groups by using the Mann-Whitney rank sum test or Bonferroni ($P < .05$ was considered statistically significant).

Results

FGF-2 Increased HDPC Proliferation

Previous studies have revealed that FGF-2 has potential ability to promote cell proliferation in a variety of cell types (28). Here we examined the effects of FGF-2 on the proliferative responses of HDPC. Fig. 1 shows that FGF-2 increased the proliferative response of HDPC in a dose-dependent manner when the cells were cultured with or without 1% FCS. FGF-2, however, has little effect on the proliferative response of HDPC that were treated with α-MEM containing 10% FCS (data not shown). FCS is essential to maintain *in vitro* cell culture especially for a long term. However, addition of FCS affects the various cell responses because FCS contains a variety of growth factors. Therefore, to minimize the effect we used 1% FCS in the proliferation and migration assays. On the other hand, 10% FCS had to be added in ALPase and alizarin staining assays to maintain the long-term culture of HDPC.

FGF-2 Suppressed Cytodifferentiation of HDPC

ALPase assay and alizarin red staining were performed to investigate the influence of FGF-2 on cytodifferentiation of HDPC. Consistent with previous findings (6, 29, 30), HDPC have potential to produce a calcified nodule with elevated levels of ALPase activity when cultured with BGP and ascorbic acid. As shown in Figs. 2, 3, and 4, FGF-2 suppressed increased levels of ALPase activity and formation of calcified nodules. Also, FGF-2 decreased ALPase activity and formation of a calcified nodule by HDPC that had been activated with ascorbic acid and BGP for 15 days. Notably, the suppressive effects of FGF-2 on both ALPase activity and calcified nodule formation were abolished when FGF-2–treated HDPC were subsequently cultured in the absence of FGF-2. This suggests that FGF-2 reversibly inhibits the differentiation of HDPC.

FGF-2 Enhanced Cell Migration

Next, we carried out the migration assay to investigate the effect of FGF-2 on cell migration of HDPC. As shown in Fig. 5, FGF-2 treatment of HDPC activated cell migration. However, it is possible that the enhanced cell migration might be caused solely by FGF-2–dependent proliferation. To exclude this possibility, HDPC were treated with MMC (the replication inhibitor), and the migration assay was then performed. First, we confirmed the inhibitory potential of MMC. Fig. 6*a* and 6*b* showed that treatment of FGF-2– or unstimulated HDPC with 16 μg/mL of MMC resulted in little proliferative response (611 ± 251 or 437 ± 109 cpm, respectively), compared with that of the cells (1727 ± 423 cpm) cultured in the absence of FCS and FGF-2. Interestingly, FGF-2 increased cell migration of HDPC that had been treated with 16 μg/mL MMC (Fig. 6*c*).

Discussion

In human dental pulp, undifferentiated mesenchymal cells are observed, as are other tissues (1, 2, 31). The stem cells can form dentin-pulp complex *in vivo* when the tissue is pathophysiologically stimulated or damaged (1). Because the proportion of undifferentiated mesenchymal cells in dental pulp is higher than that in bone marrow cells (1), it is speculated that pulp tissues possess relatively high potential to regenerate themselves. In addition, the dental pulp cells exhibit various biologic functions in response to many stimuli to maintain the homeostasis of the dentin-pulp complex (32, 33).

During tooth development, FGF-2 is present on basement membrane between oral epithelium and mesenchymal tissue (34). FGF-2 regulates differentiation of odontoblasts and ameloblasts (35) and has been reported to induce the change from preodontoblast to odontoblast, in combination with transforming growth factor–β1 or insulin-like growth factor–1 (36). These observations suggest that FGF-2 plays important roles in cytodifferentiation of odontoblasts and in dentin formation.

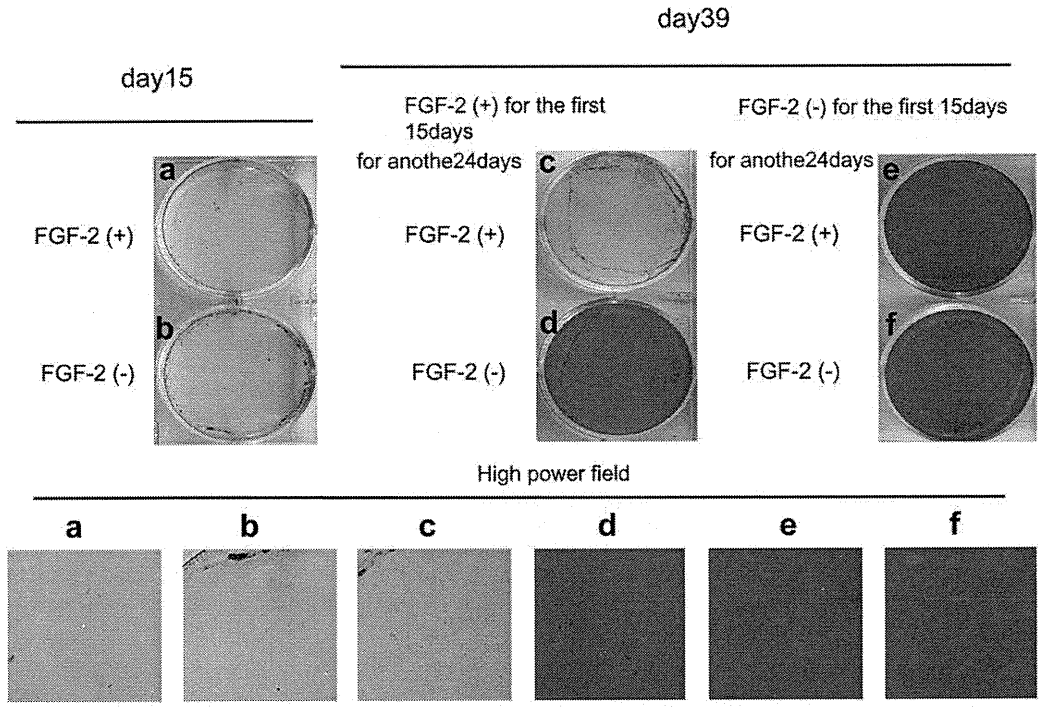

Figure 3. FGF-2 reversibly suppressed calcified nodule formation by HDPC. HDPC were cultured with standard medium containing 50 μg/mL ascorbic acid and 10 mmol/L BGP in the presence (*a*) or absence (*b*) of FGF-2 (10 ng/mL) for 15 days. The former cultures were kept in the continuous presence of FGF-2 for additional 24 days (*c*) or removed FGF-2 at the initial 15 days, after which the culture was maintained in the absence of FGF-2 (*d*). The latter culture was cultured for an additional 24 days in the absence of FGF-2 (*e*) or cultured with FGF-2 (*f*). At the end of incubation, alizarin red staining was performed. Results of 1 representative experiment among 3 identical experiments are shown.

Consistent with previous studies (37, 38), this study revealed that FGF-2 increased proliferation of HDPC (Fig. 1). Furthermore, FGF-2 activated cell migration and reversely suppressed ALPase activity and mineralization by HDPC (Figs. 2–4). The results presented in this study clearly support the hypothesis that FGF-2 modulates cell proliferation, migration, and mineralization of HDPC. FGF-2–stimulated migratory action observed in the migration assay (Fig. 5) is likely to be dependent on proliferative responses as FGF-2 has potential augmentation in DNA synthesis of HDPC (Fig. 1). Interestingly, FGF-2 stimulated migratory activity was increased even when the cell proliferation was inhibited by MMC (Fig. 6). Therefore, FGF-2 up-regulates cell migration of HDPC in addition to cell proliferative responses. Because cell proliferation and migration are critical events of wound healing and regeneration processes, cellular FGF-2–induced proliferation and migration contribute to favorable tissue repair of the dentin-pulp complex.

FGF-2 is localized in dentin and released after injury. Also, fibroblasts and endothelial cells in dental pulp produce FGF-2. Thus, HDPC

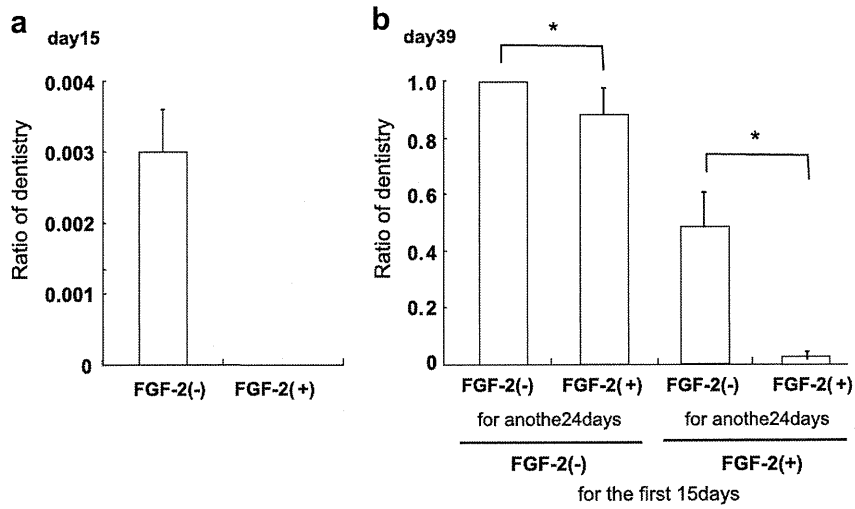

Figure 4. Quantitative evaluation on the effect of FGF-2 on calcified nodule formation by HDPC. Quantitative evaluation was determined by using image analysis with the WinRoof software program on alizarin red staining. (*a*) Results of mean and (*b*) SEM of 3 identical experiments are shown. *$P < .05$.

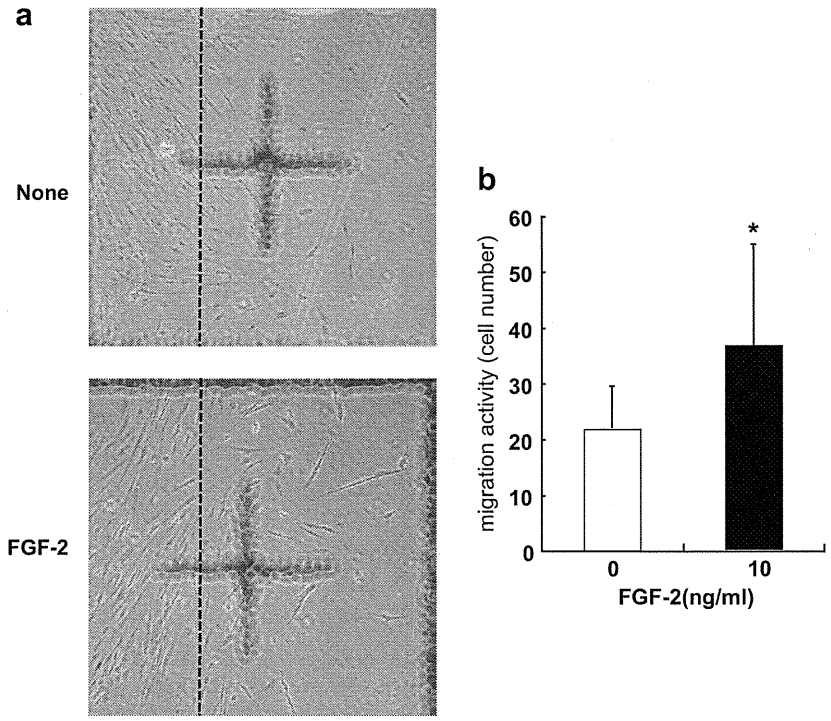

Figure 5. FGF-2 increased cell migration by HDPC. HDPC were seeded on a glass bottom dish, on which was placed a silicon block to introduce a cell-free area, and grown until confluence. The silicon block was then removed, and the medium was replaced with 1% FCS α-MEM in the presence or absence of FGF-2 (10 ng/mL). Migration of HDPC to the cleared area was photographed immediately after removing the silicon block and 24 hours later by using phase contrast microscopy. The dotted line is an edge of the cell layer just after removing silicon rubber. (*a*) Migratory activity was estimated by the assay described in Materials and Methods. (*b*) Results of mean and SEM of 3 identical experiments are shown. $*P < .05$.

are exposed to FGF-2 in physiologic and pathophysiologic conditions. HDPC expressed fibroblast growth factor receptor (FGFR) mRNA (data not shown). FGFRs are activated by its ligands such as FGF-2 and mediate cellular functions of the cells via various signaling pathways (Fig. 7).

The tissue repair process includes a sequence of functionally coordinated events involving cell proliferation and migration, release of extracellular matrix, and cytodifferentiation accompanying cell-signaling molecule interactions. Although suppression of FGF-2 for cell differentiation of HDPC was observed, HDPC, which had been pre-exposed to FGF-2 and then cultured without FGF-2, increased the ALPase activity and calcified nodule formation (Figs. 2, 3 and 4). The results emphasize the temporary suppression of differentiation by FGF-2 seen in the expanded dental pulp cells. Furthermore, HDPC are capable of cytodifferentiation at subsequent stages when other molecules distinct from FGF-2 play crucial roles. These results also suggest that FGF-2 potentiates cell growth and accumulation of HDPC that notably did not disturb cytodifferentiation of the cells later. Thus, FGF-2 is a favorable candidate for pulp capping agent.

FGF-2 enhanced pulp microvessel density (39). Revascularization is essential to wound repair. We have previously reported that FGF-2 increased hyaluronan expression by HDPC (40). Hyaluronan is capable of activating cell migration and, in turn, leads to accelerated tissue repair (41–47). Kikuchi et al (48) have demonstrated that application of FGF-2 to exposed pulp tissue leads to induced calcified particles and dentin bridge. Thus, the *in vivo* effects of FGF-2 appear to be due to multipotential actions of FGF-2 including cell proliferation, migration, and reversible suppression of cytodifferentiation observed in this study in addition to angiogenic activity and regulation of hyaluronan expression.

FGF-2 stimulates the proliferative responses but decreases the ALPase activity and mineralization of HDPC (Figs. 2, 3, and 4). At this growth stage, FGF-2 simultaneously down-regulates the mRNA expression of collagen type I, osteonectin, bone sialoprotein, DMP-1, and dentin sialophosphoprotein (data not shown), which are closely associated with the mineralization. Furthermore, the expression of decorin and biglycan is also decreased by FGF-2 (data not shown), both of which are main components of small leucin rich proteoglycan in dentin and play a critical role in mineralization of dentin and enamel (49). Thus, FGF-2–dependent modulation of extracellular matrix production can partly account for FGF-2–induced suppression of mineralization of HDPC.

Noteworthy is the fact that FGF-2–dependent inhibition of ALPase activity and calcified nodule formation was recovered when the pretreated HDPC were recultured in the absence of FGF-2 (Fig. 2 △ vs ▲; Fig. 3 (*c*) vs (*d*)). The similar phenomenon was observed when periodontal ligament cells were stimulated with FGF-2. Importantly, it has also been revealed that topical application of FGF-2 induces significant periodontal regeneration (19–21). Thus, we deduce that topically applied FGF-2 during the early stages of wound healing increases the number of progenitor cells while suppressing differentiation into hard tissue–forming cells such as osteoblasts, cementoblasts, and probably odontoblasts. During the subsequent healing processes when FGF-2 activity disappears at the applied site, those progenitor cells start to differentiate, enhancing tissue regeneration. To evaluate the efficacy of FGF-2 for regeneration of dentin-pulp complex, *in vivo* experiments with beagles are in progress.

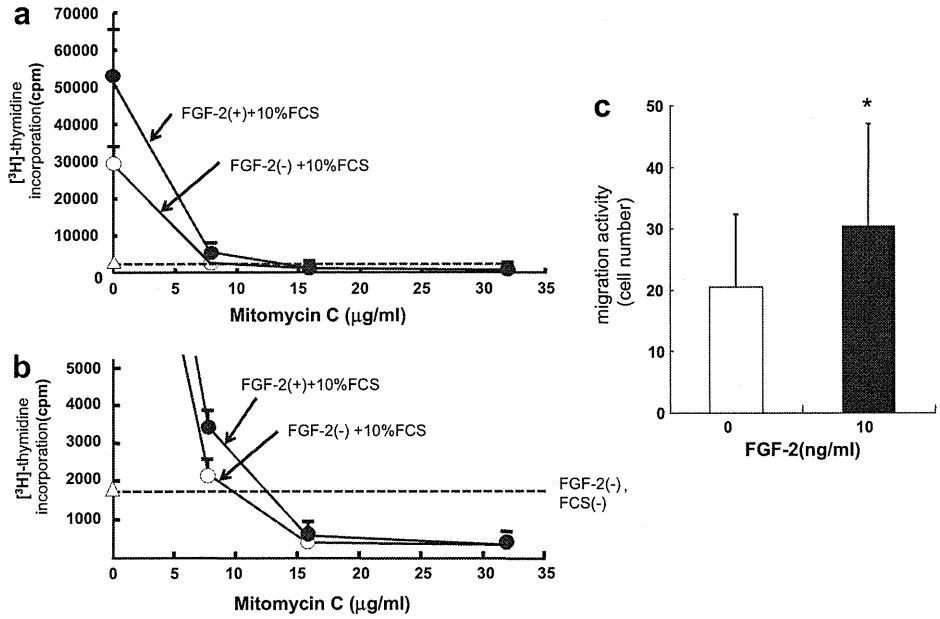

Figure 6. FGF-2 elevated cell migration by HDPC independent of cell proliferation. (*a*) HDPC were cultured with 10% FCS standard medium in 24-well culture plates to confluency and were made quiescent by culturing for 24 hours in a serum-free medium. After treatment with or without MMC for 2 hours, the cells were cultured in the presence (closed circle) or absence (open circle) of FGF-2 (10 ng/mL). HDPC were cultured in the absence of FCS, FGF-2, and MMC as a negative control (open triangle and dotted line). Proliferation was assayed by 4 hours of pulsing in wells by using [^{3}H]-thymidine. [^{3}H]-thymidine incorporation was measured in a liquid scintillation counter. Results of mean and SEM of 3 identical experiments are shown. *$P < .05$. (*b*) In this graph vertical axis is plotted as 0–5000 cpm from (*a*). (*c*) MMC-treated HDPC were seeded on a glass bottom dish, on which was placed a silicon block to introduce a cell-free area, and grown until confluence. The silicon block was then removed, and the medium was replaced with 1% FCS α-MEM in the presence or absence of FGF-2 (10 ng/mL). Migration of HDPC to the cleared area was photographed immediately after removing the silicon block and 24 hours later by using phase contrast. Migratory activity was estimated by the assay described in Materials and Methods. Results of mean and SEM of 3 identical experiments are shown. *$P < .05$.

Acknowledgments

This work was supported by a part of Grants-in-Aid for Scientific Research (no. 20592427) and the 21st Century COE entitled "Organization of Frontier BioDentistry" at Osaka University Graduate School of Dentistry supported by the Ministry of Education, Culture, Sports, Science and Technology.

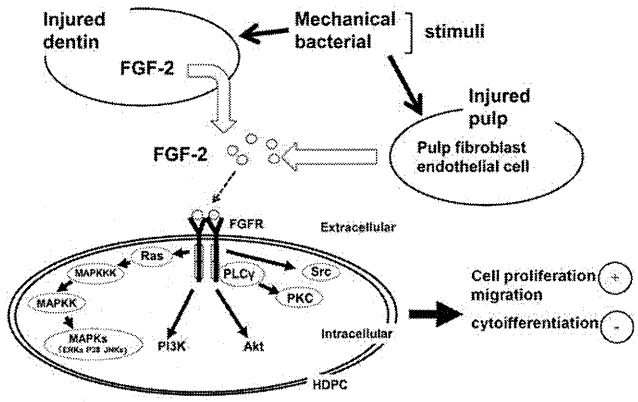

Figure 7. FGF-2 is localized in dentin and released after injury. Also, fibroblasts and endothelial cells in dental pulp produce FGF-2. Thus, HDPC are exposed to FGF-2 in physiologic and pathophysiologic conditions. HDPC expressed FGFR mRNA. FGFRs are activated by its ligands such as FGF-2 and mediate cellular functions of the cells via various signaling pathways.

References

1. Gronthos S, Mankani M, Brahim J, Robey PG, Shi S. Postnatal human dental pulp stem cells (DPSCs) in vitro and in vivo. Proc Natl Acad Sci U S A 2000;97:13625–30.
2. Gronthos S, Brahim J, Li W, et al. Stem cell properties of human dental pulp stem cells. J Dent Res 2002;81:531–5.
3. Batouli S, Miura M, Brahim J, et al. Comparison of stem-cell-mediated osteogenesis and dentinogenesis. J Dent Res 2003;82:976–81.
4. Laino G, d'Aquino R, Graziano A, et al. A new population of human adult dental pulp stem cells: a useful source of living autologous fibrous bone tissue (LAB). J Bone Miner Res 2005;20:1394–402.
5. Kuo MY, Lan WH, Lin SK, Tsai KS, Hahn LJ. Collagen gene expression in human dental pulp cell cultures. Arch Oral Biol 1992;37:945–52.
6. Tsukamoto Y, Fukutani S, Shin-Ike T, et al. Mineralized nodule formation by cultures of human dental pulp-derived fibroblasts. Arch Oral Biol 1992;37:1045–55.
7. Nakashima M, Nagasawa H, Yamada Y, Reddi AH. Regulatory role of transforming growth factor-beta, bone morphogenetic protein-2, and protein-4 on gene expression of extracellular matrix proteins and differentiation of dental pulp cells. Dev Biol 1994;162:18–28.
8. Shiba H, Fujita T, Doi N, et al. Differential effects of various growth factors and cytokines on the syntheses of DNA, type I collagen, laminin, fibronectin, osteonectin/secreted protein, acidic and rich in cysteine (SPARC), and alkaline phosphatase by human pulp cells in culture. J Cell Physiol 1998;174:194–205.
9. Buurma B, Gu K, Rutherford RB. Transplantation of human pulpal and gingival fibroblasts attached to synthetic scaffolds. Eur J Oral Sci 1999;107:282–9.
10. Buchaille R, Couble ML, Magloire H, Bleicher F. Expression of the small leucine-rich proteoglycan osteoadherin/osteomodulin in human dental pulp and developing rat teeth. Bone 2000;27:265–70.
11. Bikfalvi A, Klein S, Pintucci G, Rifkin DB. Biological roles of fibroblast growth factor-2. Endocr Rev 1997;18:26–45.
12. Nugent MA, Iozzo RV. Fibroblast growth factor-2. Int J Biochem Cell Biol 2000;32:115–20.
13. Roberts-Clark DJ, Smith AJ. Angiogenic growth factors in human dentine matrix. Arch Oral Biol 2000;45:1013–6.

14. Tran-Hung L, Laurent P, Camps J, About I. Quantification of angiogenic growth factors released by human dental cells after injury. Arch Oral Biol 2008;53:9–13.
15. Smith AJ. Pulpal responses to caries and dental repair. Caries Res 2002;36:223–32.
16. Tran-Hung L, Mathieu S, About I. Role of human pulp fibroblasts in angiogenesis. J Dent Res 2006;85:819–23.
17. McNeil PL, Muthukrishnan L, Warder E, D'Amore PA. Growth factors are released by mechanically wounded endothelial cells. J Cell Biol 1989;109:811–22.
18. Tanaka Y, Kimata K, Adams DH, Eto S. Modulation of cytokine function by heparan sulfate proteoglycans: sophisticated models for the regulation of cellular responses to cytokines. Proc Assoc Am Physicians 1998;110:118–25.
19. Takayama S, Murakami S, Shimabukuro Y, Kitamura M, Okada H. Periodontal regeneration by FGF-2 (bFGF) in primate models. J Dent Res 2001;80:2075–9.
20. Murakami S, Takayama S, Ikezawa K, et al. Regeneration of periodontal tissues by basic fibroblast growth factor. J Periodontal Res 1999;34:425–30.
21. Murakami S, Takayama S, Kitamura M, et al. Recombinant human basic fibroblast growth factor (bFGF) stimulates periodontal regeneration in class II furcation defects created in beagle dogs. J Periodontal Res 2003;38:97–103.
22. Hirano F, Hirano H, Hino E, et al. CD44 isoform expression in periodontal tissues: cell-type specific regulation of alternative splicing. J Periodontal Res 1997;32:634–45.
23. Yanagita M, Kashiwagi Y, Kobayashi R, Tomoeda M, Shimabukuro Y, Murakami S. Nicotine inhibits mineralization of human dental pulp cells. J Endod 2008;34: 1061–5.
24. Bessey OA, Lowry OH, Brock MJ. A method for the rapid determination of alkaline phosphatase with five cubic millimeters of serum. J Biol Chem 1946;164:321–9.
25. Labarca C, Paigen K. A simple, rapid, and sensitive DNA assay procedure. Anal Biochem 1980;102:344–52.
26. Dahl LK. A simple and sensitive histochemical method for calcium. Proc Soc Exp Biol Med 1952;80:474–9.
27. Smith JT, Tomfohr JK, Wells MC, Beebe TP Jr., Kepler TB, Reichert WM. Measurement of cell migration on surface-bound fibronectin gradients. Langmuir 2004;20: 8279–86.
28. Takayama S, Murakami S, Miki Y, et al. Effects of basic fibroblast growth factor on human periodontal ligament cells. J Periodontal Res 1997;32:667–75.
29. Spoto G, Fioroni M, Rubini C, Tripodi D, Di Stilio M, Piattelli A. Alkaline phosphatase activity in normal and inflamed dental pulps. J Endod 2001;27:180–2.
30. Okabe T, Sakamoto M, Takeuchi H, Matsushima K. Effects of pH on mineralization ability of human dental pulp cells. J Endod 2006;32:198–201.
31. Nakashima M, Mizunuma K, Murakami T, Akamine A. Induction of dental pulp stem cell differentiation into odontoblasts by electroporation-mediated gene delivery of growth/differentiation factor 11 (Gdf11). Gene Ther 2002;9:814–8.
32. Grando Mattuella L, Westphalen Bento L, de Figueiredo JA, Nor JE, de Araujo FB, Fossati AC. Vascular endothelial growth factor and its relationship with the dental pulp. J Endod 2007;33:524–30.
33. Smith AJ, Matthews JB, Hall RC. Transforming growth factor-beta1 (TGF-beta1) in dentine matrix: ligand activation and receptor expression. Eur J Oral Sci 1998; 106(Suppl 1):179–84.
34. Russo LG, Maharajan P, Maharajan V. Basic fibroblast growth factor (FGF-2) in mouse tooth morphogenesis. Growth Factors 1998;15:125–33.
35. Cam Y, Neumann MR, Oliver L, Raulais D, Janet T, Ruch JV. Immunolocalization of acidic and basic fibroblast growth factors during mouse odontogenesis. Int J Dev Biol 1992;36:381–9.
36. Martin A, Unda FJ, Begue-Kirn C, Ruch JV, Arechaga J. Effects of aFGF, bFGF, TGFbeta1 and IGF-I on odontoblast differentiation in vitro. Eur J Oral Sci 1998; 106(Suppl 1):117–21.
37. Nakashima M. The effects of growth factors on DNA synthesis, proteoglycan synthesis and alkaline phosphatase activity in bovine dental pulp cells. Arch Oral Biol 1992; 37:231–6.
38. Shiba H, Nakamura S, Shirakawa M, et al. Effects of basic fibroblast growth factor on proliferation, the expression of osteonectin (SPARC) and alkaline phosphatase, and calcification in cultures of human pulp cells. Dev Biol 1995;170:457–66.
39. Mullane EM, Dong Z, Sedgley CM, et al. Effects of VEGF and FGF2 on the revascularization of severed human dental pulps. J Dent Res 2008;87:1144–8.
40. Shimabukuro Y, Ueda M, Ichikawa T, et al. Fibroblast growth factor-2 stimulates hyaluronan production by human dental pulp cells. J Endod 2005;31: 805–8.
41. Comper WD, Laurent TC. Physiological function of connective tissue polysaccharides. Physiol Rev 1978;58:255–315.
42. Weigel PH, Frost SJ, McGary CT, LeBoeuf RD. The role of hyaluronic acid in inflammation and wound healing. Int J Tissue React 1988;10:355–65.
43. Oksala O, Salo T, Tammi R, et al. Expression of proteoglycans and hyaluronan during wound healing. J Histochem Cytochem 1995;43:125–35.
44. West DC, Hampson IN, Arnold F, Kumar S. Angiogenesis induced by degradation products of hyaluronic acid. Science 1985;228:1324–6.
45. Ruggiero SL, Bertolami CN, Bronson RE, Damiani PJ. Hyaluronidase activity of rabbit skin wound granulation tissue fibroblasts. J Dent Res 1987;66:1283–7.
46. Noble PW. Hyaluronan and its catabolic products in tissue injury and repair. Matrix Biol 2002;21:25–9.
47. Love SH, Shannon BT, Myrvik QN, Lynn WS. Characterization of macrophage agglutinating factor as a hyaluronic acid-protein complex. J Reticuloendothel Soc 1979; 25:269–82.
48. Kikuchi N, Kitamura C, Morotomi T, et al. Formation of dentin-like particles in dentin defects above exposed pulp by controlled release of fibroblast growth factor 2 from gelatin hydrogels. J Endod 2007;33:1198–202.
49. Goldberg M, Septier D, Rapoport O, et al. Targeted disruption of two small leucine-rich proteoglycans, biglycan and decorin, excerpts divergent effects on enamel and dentin formation. Calcif Tissue Int 2005;77:297–310.

Skeletal myoblast sheet transplantation improves the diastolic function of a pressure-overloaded right heart

Takaya Hoashi, MD,[a] Goro Matsumiya, MD, PhD,[a] Shigeru Miyagawa, MD, PhD,[a] Hajime Ichikawa, MD, PhD,[a] Takayoshi Ueno, MD, PhD,[a] Masamichi Ono, MD, PhD,[a] Atsuhiro Saito, PhD,[a] Tatsuya Shimizu, MD, PhD,[b] Teruo Okano, MD, PhD,[b] Naomasa Kawaguchi, PhD,[c] Nariaki Matsuura, MD, PhD,[c] and Yoshiki Sawa, MD, PhD[a]

Objective: The development of right ventricular dysfunction has become a common problem after surgical repair of complex congenital heart disease. A recent study reported that tissue-engineered skeletal myoblast sheet transplantation improves left ventricular function in patients with dilated and ischemic cardiomyopathy. Therefore myoblast sheet transplantation might also improve ventricular performance in a rat model of a pressure-overloaded right ventricle.

Methods: Seven-week-old male Lewis rats underwent pulmonary artery banding. Four weeks after pulmonary artery banding, myoblast sheet transplantation to the right ventricle was performed in the myoblast sheet transplantation group (n = 20), whereas a sham operation was performed in the sham group (n = 20).

Results: Four weeks after performing the procedure, a hemodynamic assessment with a pressure–volume loop showed a compensatory increase in systolic function in both groups. However, only the myoblast sheet transplantation group showed a significant improvement in the diastolic function: end-diastolic pressure (sham vs myoblast sheet transplantation, 10.3 ± 3.1 vs 5.0 ± 3.7 mm Hg; $P < .001$), time constant of isovolumic relaxation (11.1 ± 2.5 vs 7.6 ± 1.2 ms, $P < .001$), and end-diastolic pressure–volume relationship (16.1 ± 4.5 vs 7.6 ± 2.4/mL, $P < .005$). The right ventricular weight and cell size similarly increased in both groups. A histologic assessment demonstrated significantly suppressed ventricular fibrosis and increased capillary density in the myoblast sheet transplantation group in comparison with those in the sham group. Reverse transcription–polymerase chain reaction demonstrated an increased myocardial gene expression of hepatocyte growth factor and vascular endothelial growth factor in the myoblast sheet transplantation group but not in the sham group.

Conclusions: Skeletal myoblast sheet transplantation improved the diastolic dysfunction and suppressed ventricular fibrosis with increased capillary density in a rat model of a pressure-overloaded right ventricle. This method might become a novel strategy for the myocardial regeneration of right ventricular failure in patients with congenital heart disease.

Because of recent developments in diagnostic methods, the establishment of new surgical techniques, and improvements in perioperative management, patients with complex congenital heart disease (CHD) are today often able to survive to adulthood. However, even after a successful repair, right ventricular (RV) overload remains in some patients, in whom it impairs RV function and influences long-term mortality and morbidity.[1-3] Chronic pressure overload is one of the major risk factors of RV dysfunction. In this situation the right ventricle is hypertrophied and systolic function is initially preserved, whereas diastolic function gradually deteriorates.[4,5] Prolonged exposure to excessive pressure overload results in irreversible RV failure. Clinically, the relationship between progressive fibrosis and RV function must be addressed.[6-8]

Recently, cardiac regeneration therapy has provided a new treatment for end-stage heart failure, and skeletal myoblasts are currently thought to be a potential cell source.[9-11] We developed a novel cell delivery system using temperature-responsive culture dishes,[12] and tissue-engineered cell sheets have been created without any scaffold, which maintains cell–cell interaction and extracellular matrix while avoiding any inflammatory reaction, and with improved cell survival.[13] Skeletal myoblast sheet transplantation (MST) has been shown to improve left ventricular (LV) contractility in several animal models of LV failure.[14-16] Otherwise, it is unclear whether MST can also affect the right ventricle, especially pressure-induced RV dysfunction. Hence this study assessed whether MST could improve RV function in rats after damage caused by pressure overload.

From the Department of Cardiovascular Surgery,[a] Osaka University Graduate School of Medicine, Osaka, Japan; the Institute of Advanced Biomedical Engineering and Science,[b] Tokyo Women's Medical University, Tokyo, Japan; and the Department of Molecular Pathology,[c] Osaka University Graduate School of Allied Health Science, Osaka, Japan.

Received for publication March 17, 2008; revisions received Oct 1, 2008; accepted for publication Feb 2, 2009.

Address for reprints: Yoshiki Sawa, MD, PhD, 2–2 Yamadaoka, Suita, Osaka 565-0871, Japan (E-mail: sawa@surg1.med.osaka-u.ac.jp).

J Thorac Cardiovasc Surg 2009;138:460-7
0022-5223/$36.00

doi:10.1016/j.jtcvs.2009.02.018

Abbreviations and Acronyms

BW = body weight
CFR = coronary flow reserve
EDPVR = end-diastolic pressure–volume relationship
Ees = end-systolic elastance
ESPVR = end-systolic pressure–volume relationship
GAPDH = glyceraldehyde-3-phosphate dehydrogenase
HGF = hepatocyte growth factor
IVS = intraventricular septum
LV = left ventricular
MS = myoblast cell sheet
MST = myoblast sheet transplantation
PA = pulmonary artery
PAB = pulmonary artery banding
PRSW = preload recruitable stroke work
RT-PCR = reverse transcription–polymerase chain reaction
RV = right ventricular
SW = stroke work
VEGF = vascular endothelial growth factor

MATERIALS AND METHODS

Animal Care

All experimental procedures and protocols used in this investigation were reviewed and approved by the institutional animal care and use committee and are in accordance with the National Institutes of Health "Guide for the care and use of laboratory animals" (National Institutes of Health publication no. 85-23, revised 1996).

Creation of Chronic RV Pressure Overload

A rat model of pulmonary artery banding (PAB) was established to create chronic RV pressure overload. Seven-week-old male Lewis rats (180–210 g) were anesthetized with an intraperitoneal injection of ketamine hydrochloride (50 mg/kg) and xylazine (5 mg/kg) and ventilated by using a volume-controlled respirator (2 mL, 60 cycles/min) with room air. A left thoracotomy was performed at the fourth intracostal space, and the main pulmonary artery (PA) was carefully exposed. As previously reported,[17] a 19-gauge injection needle (outer diameter, 1.1 mm) was placed alongside the PA, and a 3-0 polyester suture was tied tightly around the PA and the needle. Next, the needle was rapidly removed, and then a fixed diameter was set for the PA. Thereafter, the thorax was closed in layers, and the ventilator setting was changed (90 cycles/min) for half an hour to reduce the respiratory load.

Skeletal Myoblast Sheet Preparation

Creation of myoblast cell sheets (MSs) with temperature-responsive culture dishes (UpCell; Cellseed, Tokyo, Japan) was done according to previous reports.[14-16] Briefly, skeletal muscle was harvested from the hind legs of 4-week-old syngeneic rats. The purified myoblasts were incubated on 35-mm UpCell dishes at 37°C, with the cell numbers adjusted to 3×10^6 per dish. After 12 to 18 hours, the dishes were moved to a refrigerator set at 20°C and left there for 30 minutes. During that time, the MSs detached spontaneously from the surfaces. Each sheet measured from 10 to 15 mm in diameter.

Skeletal MST

Four weeks after PAB, a second left thoracotomy was performed at the fifth intracostal space after achievement of general anesthesia. After opening the pericardium, the RV anterior wall was exposed. Two MSs were grafted onto each anterior wall of the right ventricle in the MST group (n = 20), or a sham operation was performed in the sham group (n = 20). The pericardium was closed linearly before the thorax was closed to prevent the dislocation of MSs. In addition, age-matched rats that did not undergo surgical intervention were also prepared as a control group (n = 20).

Hemodynamic Study and Data Analysis

Four weeks after the MST or sham operation, 10 rats in each group were anesthetized and ventilated again and were set on the blanket warmer to maintain body temperature. A median sternotomy was performed, and the pericardium was opened carefully to minimize hemorrhaging. A silk thread was placed under the inferior vena cava just above the diaphragm to change the RV preload. After purse-string sutures were attached with 7-0 polypropylene, the conductance catheter (Unique Medical Co, Tokyo, Japan) was inserted through the RV apex toward the pulmonary valve along the longitudinal axis of the RV cavity and then fixed. A Miller 1.4F pressure-tip catheter (SPR-719; Millar Instruments, Houston, Tex) was also inserted from the RV anterior wall and fixed. For better volume measurement, a 1-mm curve was added to the original standard straight conductance catheter to fit the complex RV geometry. The position of the conductance catheter was determined by observing the pressure and segmental volume signals with the appropriate phase relationships. The conductance system and the pressure transducer controller (Integral 3 [VPR-1002], Unique Medical Co) were set as previously reported.[18] Pressure–volume loops and intracardiac electrocardiograms were monitored online, and the conductance, pressure, and intracardiac electrocardiographic signals were analyzed with Integral 3 software (Unique Medical Co).[18]

Under stable hemodynamic conditions, the baseline indices were initially measured, and then the pressure–volume loop was drawn during inferior vena caval occlusion and analyzed (Figure 1). Finally, the conductivity of the sampled blood was measured with a small (0.1 mm) cuvette, and the parallel conductance volume was measured with the hypertonic saline dilution method to obtain the absolute volumes.[19]

The following indices were calculated as the baseline RV function: heart rate, end-systolic pressure, end-diastolic pressure, dP/dtmax, dP/dtmin, and the time constant of isovolumic relaxation (τ). The following relationships were determined by means of pressure–volume loop analysis as load-independent measures of RV function: end-systolic pressure–volume relationship (ESPVR), end-diastolic pressure–volume relationship (EDPVR), and preload recruitable stroke work (PRSW).

The ESPVR is linear, and it can be characterized by a slope (end-systolic elastance [Ees]) and a volume axis intercept (Vo), so that $Pes = Ees(Ves–Vo)$, where Pes and Ves are the end-systolic pressure and volume, respectively.[20]

In contrast, the EDPVR is intrinsically thought to be nonlinear. The relationship between the end-diastolic pressure (Ped) and volume (Ved) can be fitted to the monoexponential, so that $Ped = Po+be^{KvVed}$, where Po is the pressure asymptote (generally close to 0 mm Hg), b is a constant, and Kv is the variable represented as a ventricular stiffness property.[21]

The relationship between ventricular stroke work (SW) and end-diastolic volume (Ved) is represented as PRSW. PRSW is thought to be a suitable parameter of the contractile state and fitted to the following equation: $SW = K(Ved–Vo)$, where K is a constant as a potential measure of intrinsic myocardial performance independent of loading, geometry, and heart rate.[22]

Histopathologic Analysis

The other 10 rats in each group were killed 4 weeks after the sham or MST operation for histologic analysis, reverse transcription–polymerase chain reaction (RT-PCR), and blood sampling. The hearts were quickly removed, and the ventricles were dissected free of atrial tissue and large

ET/BS

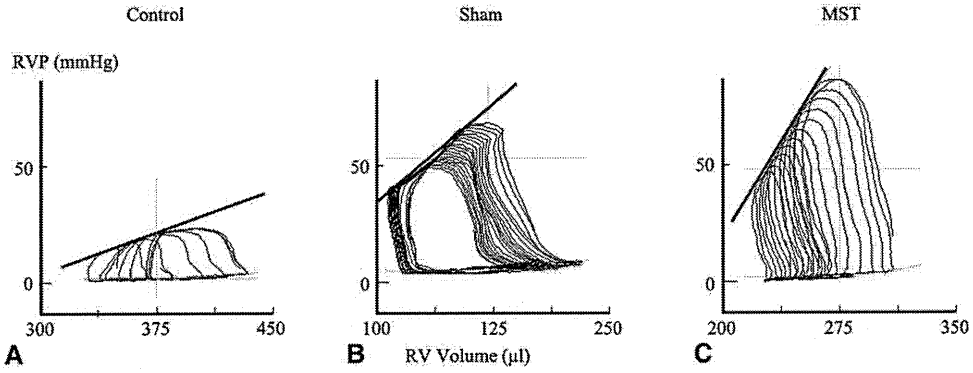

FIGURE 1. Representative pressure–volume loops of the control (A), sham (B), and myoblast sheet transplantation (*MST*; C) groups under different loading conditions. The slope of the end-systolic pressure–volume relationship is displayed as a *black straight line*. The correlation of the end-diastolic pressure–volume relationship is displayed as a *green monoexponential curve*. *RVP*, Right ventricular pressure; *RV*, right ventricle.

blood vessels. The right ventricle was carefully separated from the left ventricle and intraventricular septum (IVS). The fresh ventricular tissues were immediately blotted dry and weighted separately to determine the degree of RV hypertrophy based on 2 parameters: RV wall weight/body weight (RV/BW) and RV wall weight/LV and IVS wall weight (RV/LV+IVS).

Tissue specimens were obtained from the endocardium, the midwall, and the epicardium of the RV anterior wall in cross-sections, cut into 5-μm-thick sections, and stained with hematoxylin and eosin for morphologic analysis, including measurement of RV wall thickness, periodic acid–Schiff staining to measure the short-axis length of the RV myocardial cell, Factor VIII–related antigen staining (Dako EPOS anti-human Von Willebrand factor/HRP; Dako Cytomation, Glostrup, Denmark) to quantify capillary vascular density, and Masson trichrome staining for determination of the amount of interstitial and myocardial fibrosis. The percentage of interstitial and myocardial fibrosis were assessed by a computer-based method[23,24] with the use of a software filter (Mac Scope Software; MITANI Corp, Tokyo, Japan), which can recognize the distinct color shades. The number of pixels of the blue-stained collagen area was calculated, then divided by the total number of pixels in a field. Each 3 fields of the endocardial, epicardial, and mid layers of the RV wall per slide were analyzed and then averaged.

RT-PCR

Total RNA was isolated from the stored specimens by using the RNeasy Mini Kit (Qiagen, Hilden, Germany) and reverse transcribed with Omniscript Reverse Transcriptase (Qiagen). RT-PCR was performed with the ABI PRISM 7700 (Applied Biosystems, Foster City, Calif). Measurement of the mRNA expression of hepatocyte growth factor (HGF) and vascular endothelial growth factor (VEGF) was performed in triplicate. The results are expressed after normalization for glyceraldehyde-3-phosphate dehydrogenase (GAPDH).

Statistical Analysis

All data were expressed as the mean ± SEM and range. Student's unpaired *t* test or analysis of variance for parametric values was used to compare group means.

RESULTS

Pressure Overload and Hypertrophy of the Right Ventricle After PAB

After PAB, a weight analysis showed the heart weight/BW, RV/BW, and RV/(LV+IVS) weight ratios in the sham and MST groups to be similar and significantly higher than in the control group (Table 1). Both the sham and MST groups showed a significantly increased end-systolic pressure and dP/dtmax than seen in the control group (Table 2).

Hemodynamic Effects of MST

The baseline indices revealed that end-diastolic pressure and τ values were significantly increased only in the sham group in comparison with those in the control group but not in the MST group (Table 2). Typical examples of the pressure–volume loop in each group are presented in Figure 1. The pressure–volume loop analysis revealed that the ESPVR and PRSW values significantly increased both in the sham and MST groups. However, the EDPVR value significantly increased only in the sham group (control vs sham vs MST groups: 8.6 ± 2.9 vs 16.1 ± 4.5 vs 7.6 ± 2.4/mL; $P < .05$ in the control and MST groups vs the sham group; Table 2).

Histologic Effects of MST

Whole heart findings showed the RV wall thickened, the cavity enlarged, and the IVS shifted toward the left side in the sham and MST groups (Figure 2, *A*). In the MST group transplanted MSs were observed as an elastic thin layer on the epicardium (Figure 2, *B*). The RV wall thickness and myocardial cell size in the sham and MST groups were similar and significantly higher than in the control group (Figure 2, *C–E*).

TABLE 1. Weight analysis at the fourth week after the operation

Group	Control	Sham	MST
HW/BW (mg/g)	2.62 ± 0.09	3.53 ± 0.50*	4.03 ± 0.59*
RV/BW (mg/g)	0.54 ± 0.15	1.62 ± 0.42*	1.65 ± 0.32*
RV/(IVS+LV)	0.27 ± 0.08	0.69 ± 0.11*	0.69 ± 0.09*

MST, Myoblast sheet transplantation; *HW*, heart weight; *BW*, body weight; *RV*, right ventricle; *IVS*, interventricular septum; *LV*, left ventricle. *$P < .05$ versus the control group.

TABLE 2. Hemodynamic indices at the fourth week after the operation

Group	Control	Sham	MST
Basic hemodynamic indices			
HR (beats/min)	280 ± 72	233 ± 34	249 ± 65
ESP (mm Hg)	22.8 ± 2.9	82.3 ± 11.8*	78.7 ± 13.2*
EDP (mm Hg)	2.4 ± 1.4	10.3 ± 3.1*†	5.0 ± 3.7
dP/dtmax (mm Hg/s)	1301 ± 206	3197 ± 597*	3352 ± 1332*
dP/dtmin (mm Hg/s)	–997 ± 210	–2466 ± 582*	–2682 ± 828*
τ (ms)	7.9 ± 2.7	11.1 ± 2.5*†	7.6 ± 1.2
Load-independent parameters analyzed by PV loop			
ESPVR (mm Hg/mL)	538 ± 196	857 ± 305*	967 ± 201*
EDPVR (/mL)	8.6 ± 2.9	16.1 ± 4.5*†	7.6 ± 2.4
PRSW (mm Hg)	17.0 ± 4.1	40.2 ± 19.6*	40.8 ± 13.6*
PRSW/RV (mm Hg/kg)	88.3 ± 23.9	71.5 ± 31.3	73.6 ± 28.8

MST, Myoblast sheet transplantation; *HR*, heart rate; *ESP*, end-systolic pressure; *EDP*, end-diastolic pressure; *PV*, pressure–volume; *ESPVR*, end-systolic pressure–volume relationship; *EDPVR*, end-diastolic pressure–volume relationship; *PRSW*, preload-recruitable stroke work; *RV*, right ventricular weight. *$P < .05$ versus the control group. †$P < .05$ versus the MST group.

Factor VIII stain showed that myocardial capillary vascular density showed no significant difference at the mid layer and endocardial layer (Figure 3, *B* and *C*), but it was significantly higher in the MST group than in the other 2 groups at the epicardial layer (Figure 3, *A*). Hence, total capillary density in the MST group was significantly higher than in the other 2 groups (control vs sham vs MST groups: 262 ± 98 vs 271 ± 289 vs 823 ± 708; $P < 0.05$ in the control and sham groups vs the MST group; Figure 3, *D*).

Periodic acid–Schiff staining demonstrated significant interstitial fibrosis of the right ventricle in both the sham and MST groups, but the percentage of fibrosis in the

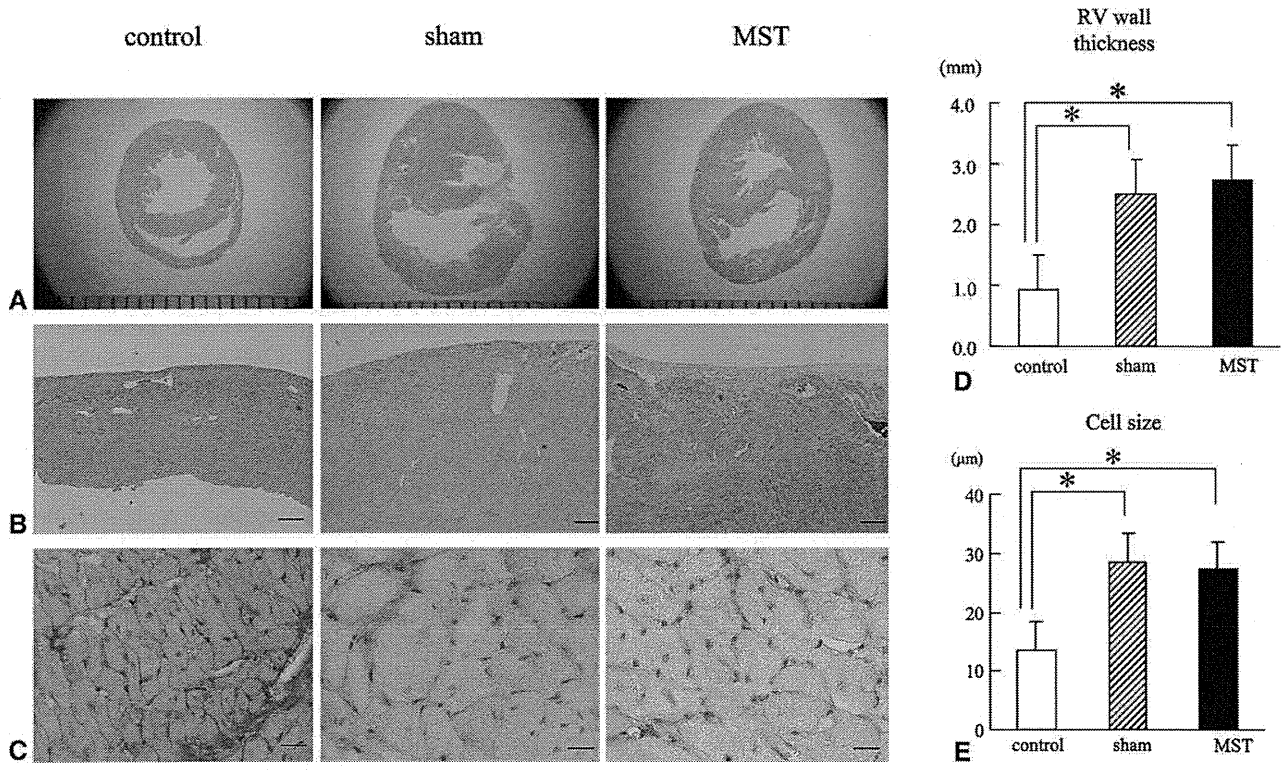

FIGURE 2. Macroscopic photographs of hematoxylin and eosin–stained sections showing right ventricular *(RV)* wall thickening, cavity enlarging, and the intraventricular septum shifting towered the left side in the sham and myoblast sheet transplantation *(MST)* groups (A and D). Photomicrographs (40×, scale bar = 200 μm) of hematoxylin and eosin–stained sections showed a fibrous organized thin layer on the epicardium in the myoblast sheet transplantation group (B). Photomicrographs (400×, scale bar = 20 μm) of periodic acid–Schiff–stained sections showed significantly hypertrophied ventricular myocytes in the sham and myoblast sheet transplantation groups (C and E). *$P < .05$ (n = 10).

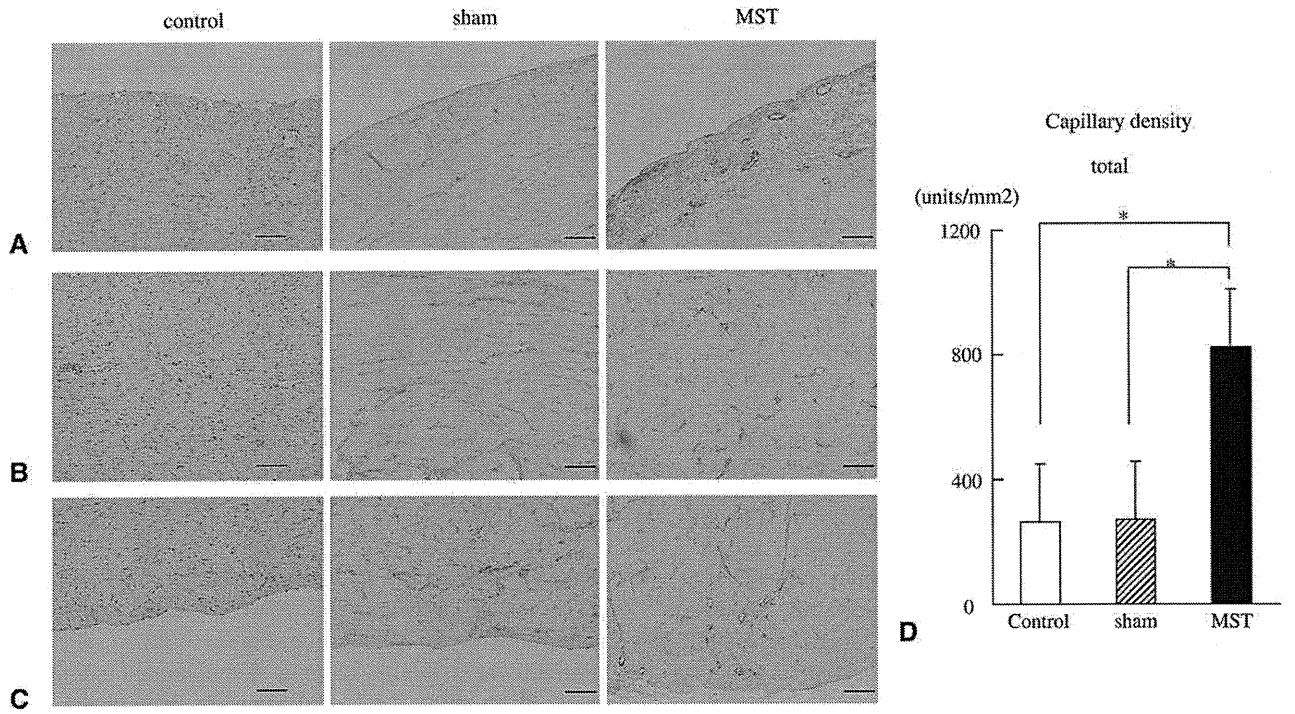

FIGURE 3. Representative photomicrographs (100×, scale bar = 100 μm) of Factor VIII–stained epicardial layer (A), mid layer (B), and endocardial layer (C). Neovascularization occurred at the epicardial layer in the myoblast sheet transplantation *(MST)* group (D). *$P < .05$ (n = 10).

MST group was significantly less than that in the sham group (control vs sham vs MST groups: 4.8% ± 1.1% vs 24.5% ± 10.0% vs 19.0% ± 5.1%; $P < .05$ between each 2 groups; Figure 4, *A* and *E*). Aggregated endomyocardial fibrosis was detected only in the sham group (endomyocardial percentage of fibrosis, control vs sham vs MST groups: 5.7% ± 0.1% vs 31.5% ± 8.4% vs 18.6% ± 5.9%; $P < .01$ in the control and MST groups vs the sham group; Figure 4, *B–D* and *F*).

RT-PCR

The expression of HGF and VEGF mRNA in the MST group was significantly higher than in the sham group (control vs sham vs MST groups: HGF, 0.00009 ± 0.00008 vs 0.00041 ± 0.00030 vs 0.00073 ± 0.00031/GAPDH [$P < .05$ in each group]; *VEGF*, 0.00242 ± 0.00164 vs 0.00329 ± 0.00181 vs 0.00512 ± 0.00113/GAPDH [$P < .05$ in the control and sham group vs the MST group]; Figure 5).

DISCUSSION

This study demonstrated that skeletal MST improved diastolic function in a pressure-overloaded right heart model in rats by means of PAB. This conclusion is supported by the following evidence: (1) the diastolic function was significantly improved based on hemodynamic assessment and pressure–volume loop analysis; (2) interstitial and endocardial fibrosis was ameliorated, and capillary vascular density of the epicardial layer was increased; and (3) myocardial gene expression of HGF and VEGF was significantly increased. MST has been shown to have therapeutic effects in several models of LV failure.[14-16] However, the present results are the first to show evidence that MST is effective for the treatment of RV dysfunction resulting from chronic pressure overload.

Prolonged RV pressure overload promotes unique morphologic, histologic, and functional changes. The mechanical stimulation of pressure overload extends the myocardium, which leads to diastolic dysfunction.[21] Simultaneously, hypertrophied myocardium upregulates the release of various chemical mediators,[17] which induce further myocardial expansion, apoptosis, necrosis, and fibrosis, finally resulting in RV decompensation. Otherwise, ventricular hypertrophy itself reduces the coronary flow reserve (CFR) and leads to coronary microcirculatory dysfunction.[25] As studies on the left ventricle show, this phenomenon is detected particularly in the subendocardium.[26] The shortage of CFR induces myocardial cellar mortality and endocardial fibrosis, which accelerates ventricular dysfunction. The present and previous data indicate that transplanted elastic cells initially improved ventricular stiffness[14] and preserved CFR in the hypertrophied myocardium, both of which generate a synergistic effect of the suppression of myocardial cell death and fibrosis, especially at the endocardial layer. Although an angiogenetic effect was observed with the increased myocardial gene expression of HGF and VEGF, we speculate this does not increase endocardial coronary flow directly because increased

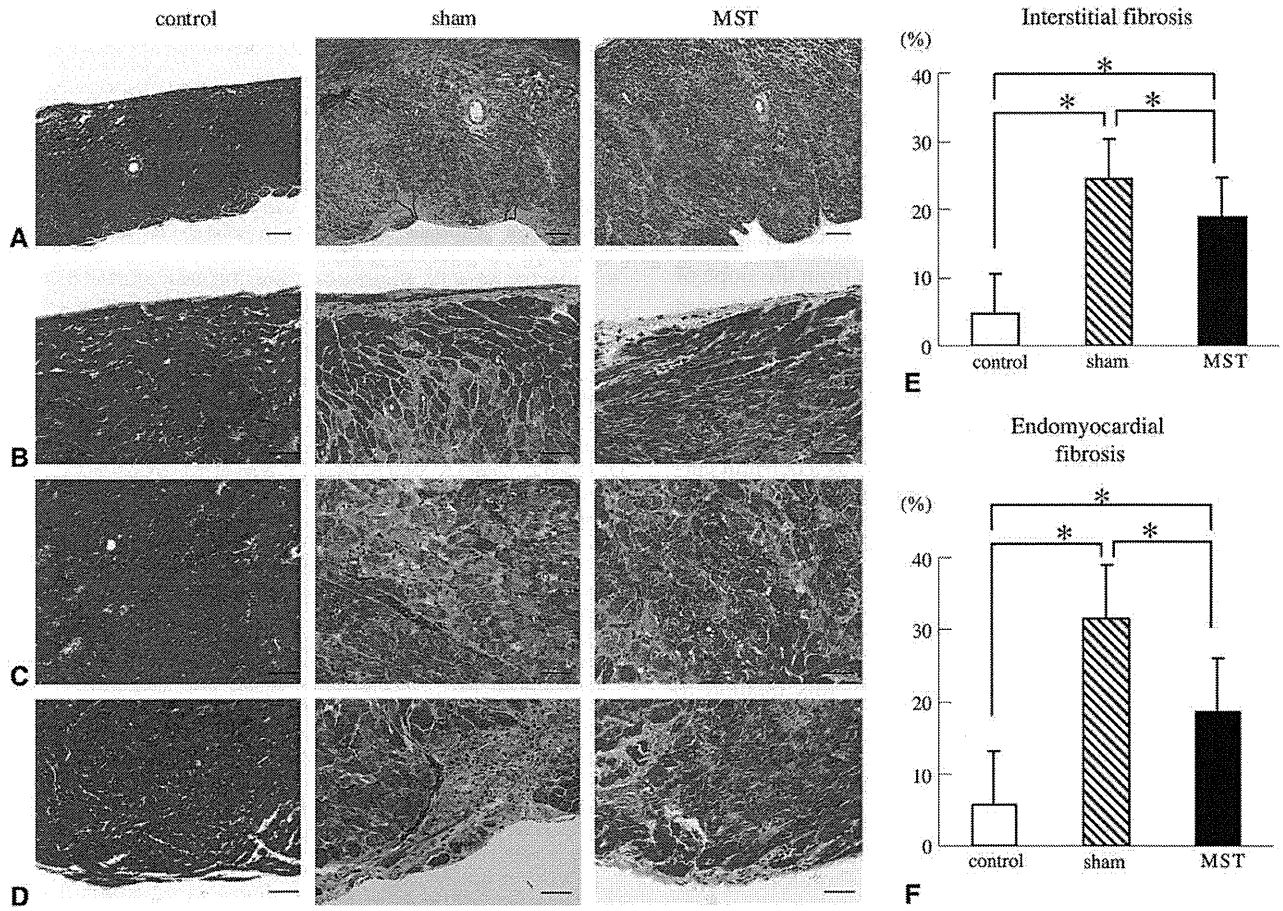

FIGURE 4. Representative photomicrographs of Masson's trichrome–stained transmural layer (A; 40×, scale bar = 200 μm), epicardial layer (B), mid layer (C), and endocardial layer (D; 200×, scale bar = 50 μm) for evaluation of interstitial (E) and endomyocardial (F) fibrosis. *$P < .05$ (n = 10).

capillary density was only seen at epicardial layer. These new capillaries might increase the blood supply to the transplanted myoblasts and prolong their survival.[13]

As several LV studies have previously shown, Lamberts and colleagues[27] revealed the strict relationship between RV chamber stiffness and the degree of myocardial fibrosis. In their report they also described that prevention or reduction of RV fibrosis improved RV diastolic dysfunction. Although we could not show any individual correlation between collagen contents and hemodynamic parameters in regard to diastolic function, these findings strongly support our results. Therefore we would like to emphasize that the suppression of fibrosis improved the RV diastolic function.

The hemodynamic assessment of cardiac performance of a hypertrophied right ventricle has not been established. Various attempts have been made; however, it is still necessary to perform cardiac catheterization to evaluate hemodynamics, especially regarding diastolic function.[28,29] Leeuwenburgh and associates[4] showed that RV compliance deteriorated in a lamb model and described τ and EDPVR values to be useful indicators for diastolic function. Gaynor

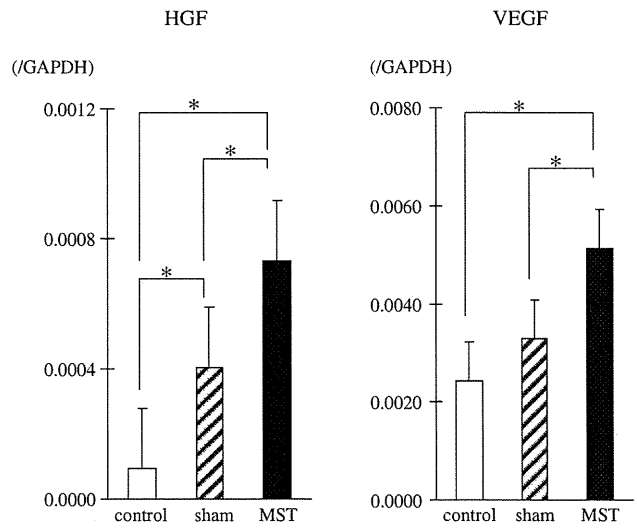

FIGURE 5. RT-PCR for evaluation of neurohormonal factor gene expression. The results are expressed after normalization for GAPDH. *HGF*, Hepatocyte growth factor; *VEGF*, vascular endothelial growth factor. *$P < .05$ (n = 10).

and coworkers[5] also showed an increase of EDPVR in a dog model of PAB. The current results are consistent with these reports. Therefore these data appear to be reliable.

On the other hand, the assessment of systolic function still remains controversial. In this study we showed that ESPVR (Ees) and PRSW were significantly increased in sham groups, as previously reported.[30] However, Dell'Italia and Walsh[31] pointed out that in the assessment of RV contractility, the slope of ESPVR (Ees) was different from the slope of the maximum time-varying elastance, which better reflected the RV contractility than Ees. In addition to Ees, PRSW is thought to be an optimal parameter of ventricular contractility. However, we might have to consider the discrepancy of the cardiac mass between normal and hypertrophied hearts because ventricular SW should be assessed as a per-unit cardiac mass. We tried to calculate the PRSW divided for each animal's RV weight, which revealed there was no statistical significance among the 3 groups (control vs sham vs MST groups: 88.3 ± 23.9 vs 71.5 ± 31.3 vs 73.6 ± 28.8 mm Hg/kg, Table 2). Hence it is hard to say that the RV pressure load induced a further improvement in RV contractility.

We need further investigation to apply this method to clinical RV failure because we did not ascertain the effect of MST on RV systolic function. Nevertheless, enormous fibrosis was seen in the sham group, and systolic function was still compensated until the timing of hemodynamic evaluation. However, previous reports showed that MST had an excellent effect on LV contractility.[14-16] Therefore we expect that this method might become a novel and potentially effective treatment strategy for patients with RV failure.

In conclusion, chronic pressure overload to the right ventricle caused hypertrophy and impaired diastolic function in rats. Skeletal MST attenuated diastolic dysfunction, which was mainly caused by suppressed interstitial and endocardial fibrosis. This method might become a novel strategy for the myocardial regeneration of RV failure in patients with CHD in the future.

We thank Mrs Masako Yokoyama for her expert assistance with RT-PCR and Kazuhiro Takekita and Takeshi Miki for technical support in creating the tissue-engineered skeletal MSs.

References

1. Bolger AP, Coats AJ, Gatzoulis MA. Congenital heart disease: the original heart failure syndrome. *Eur Heart J.* 2003;24:970-6.
2. Murphy JG, Gersh BJ, Mair DD, Fuster V, McGoon MD, Ilstrup DM, et al. Long-term outcome in patients undergoing surgical repair of tetralogy of Fallot. *N Engl J Med.* 1993;329:593-9.
3. Gatzoulis MA, Balaji S, Webber SA, Siu SC, Hokanson JS, Poile C, et al. Risk factors for arrhythmia and sudden cardiac death late after repair of tetralogy of Fallot: a multicentre study. *Lancet.* 2000;356:975-81.
4. Leeuwenburgh BP, Steendijk P, Helbing WA, Baan J. Indexes of diastolic RV function: load dependence and changes after chronic RV pressure overload in lambs. *Am J Physiol Heart Circ Physiol.* 2002;282:1350-8.
5. Gaynor SL, Maniar HS, Bloch JB, Steendijk P, Moon MR. Right atrial and ventricular adaptation to chronic right ventricular pressure overload. *Circulation.* 2005;112:212-8.
6. Deanfield JE, Ho SY, Anderson RH, McKenna WJ, Allwork SP, Hallidie-Smith KA. Late sudden death after repair of tetralogy of Fallot: a clinicopathologic study. *Circulation.* 1983;67:626-31.
7. Babu-Narayan SV, Kilner PJ, Li W, Moon JC, Goktekin O, Davlouros PA, et al. Ventricular fibrosis suggested by cardiovascular magnetic resonance in adults with repaired tetralogy of Fallot and its relationship to adverse markers of clinical outcome. *Circulation.* 2006;113:405-13.
8. Chowdhury UK, Sathia S, Ray R, Singh R, Pradeep KK, Venugopal P. Histopathology of the right ventricular outflow tract and its relationship to clinical outcomes and arrhythmias in patients with tetralogy of Fallot. *J Thorac Cardiovasc Surg.* 2006;132:270-7.
9. Taylor DA, Atkins BZ, Hungspreugs P, Jones TR, Reedy MC, Hutcheson KA, et al. Regenerating functional myocardium: improved performance after skeletal myoblast transplantation. *Nat Med.* 1998;4:929-33.
10. Menasche P, Hagege AA, Scorsin M, Pouzet B, Desnos M, Duboc D, et al. Myoblast transplantation for heart failure. *Lancet.* 2001;357:279-80.
11. Hagege AA, Marolleau JP, Vilquin JT, Alheritiere A, Peyrard S, Duboc D, et al. Skeletal myoblast transplantation in ischemic heart failure: long-term follow-up of the first phase I cohort of patients. *Circulation.* 2006;114:108-13.
12. Okano T, Yamada N, Sakai H, Sakurai Y. A novel recovery system for cultured cells using plasma-treated polystyrene dishes grafted with poly(N-isopropylacrylamide). *J Biomed Mater Res.* 1993;27:1243-51.
13. Miyagawa S, Sawa Y, Sakakida S, Taketani S, Kondoh H, Memon IA, et al. Tissue cardiomyoplasty using bioengineered contractile cardiomyocyte sheets to repair damaged myocardium: their integration with recipient myocardium. *Transplantation.* 2005;80:1586-95.
14. Memon IA, Sawa Y, Fukushima N, Matsumiya G, Miyagawa S, Taketani S, et al. Repair of impaired myocardium by means of implantation of engineered autologous myoblast sheets. *J Thorac Cardiovasc Surg.* 2005;130:1333-41.
15. Kondoh H, Sawa Y, Miyagawa S, Sakakida-Kitagawa S, Memon IA, Kawaguchi N, et al. Longer preservation of cardiac performance by sheet-shaped myoblast implantation in dilated cardiomyopathic hamsters. *Cardiovasc Res.* 2006;69:466-75.
16. Hata H, Matsumiya G, Miyagawa S, Kondoh H, Kawaguchi N, Matsuura N, et al. Grafted skeletal myoblast sheets attenuate myocardial remodeling in pacing-induced canine heart failure model. *J Thorac Cardiovasc Surg.* 2006;132:918-24.
17. Lekanne Deprez RH, van den Hoff MJ, de Boer PA, Ruijter PM, Maas AA, Chamuleau RA, et al. Changing patterns of gene expression in the pulmonary trunk-banded rat heart. *J Mol Cell Cardiol.* 1998;30:1877-88.
18. Sato T, Shishido T, Kawada T, Miyano H, Miyashita H, Inagaki M, et al. ESPVR of in situ rat left ventricle shows contractility-dependent curvilinearity. *Am J Physiol Heart Circ Physiol.* 1998;274:H1429-34.
19. Baan J, van der Velde ET, de Bruin HG, Smeenk GJ, Koops J, van Dijk AD, et al. Continuous measurement of left ventricular volume in animals and humans by conductance catheter. *Circulation.* 1984;70:812-23.
20. Suga H, Sagawa K. Instantaneous pressure-volume relationships and their ratio in the excised, supported canine left ventricle. *Circ Res.* 1974;35:117-26.
21. Gaasch WH, Cole JS, Quinones MA, Alexander JK. Dynamic determinants of left ventricular diastolic pressure-volume relations in man. *Circulation.* 1975;51:317-23.
22. Glower DD, Spratt JA, Snow ND, Kabas JS, Davis JW, Olsen CO, et al. Linearity of the Frank-Starling relationship in the intact heart: the concept of preload recruitable stroke work. *Circulation.* 1985;71:994-1009.
23. Hoyt RH, Collins SM, Skorton DJ, Ericksen EE, Conyers D. Assessment of fibrosis in infarcted human hearts by analysis of ultrasonic backscatter. *Circulation.* 1985;71:740-4.
24. Vasiljević JD, Popović ZB, Otasević P, Popović ZV, Vidaković R, Mirić M, et al. Myocardial fibrosis assessment by semiquantitative, point-counting and computer-based methods in patients with heart muscle disease: a comparative study. *Histopathology.* 2001;38:338-43.
25. Murray PA, Vatner SF. Reduction of maximal coronary vasodilator capacity in conscious dogs with severe right ventricular hypertrophy. *Circ Res.* 1981;48:25-33.
26. Rajappan K, Rimoldi OE, Dutka DP, Ariff B, Pennell DJ, Sheridan DJ, et al. Mechanisms of coronary microcirculatory dysfunction in patients with aortic stenosis and angiographically normal coronary arteries. *Circulation.* 2002;105:470-6.
27. Lamberts RR, Caldenhoven E, Lansink M, Witte G, Vaessen RJ, St Cyr JA, et al. Preservation of diastolic function in monocrotaline-induced right ventricular hypertrophy in rats. *Am J Physiol Heart Circ Physiol.* 2007;293:H1869-76.

28. Haddad F, Hunt SA, Rosenthal DN, Murphy DJ. Right ventricular function in cardiovascular disease, part I: anatomy, physiology, aging, and functional assessment of the right ventricle. *Circulation*. 2008;117:1436-48.
29. Burkhoff D, Mirsky I, Suga H. Assessment of systolic and diastolic ventricular properties via pressure-volume analysis: a guide for clinical, translational, and basic researchers. *Am J Physiol Heart Circ Physiol*. 2005;289:H501-12.
30. Faber MJ, Dalinghaus M, Lankhuizen IM, Steendijk P, Hop WC, Schoemaker RG, et al. Right and left ventricular function after chronic pulmonary artery banding in rats assessed with biventricular pressure-volume loops. *Am J Physiol Heart Circ Physiol*. 2006;291:H1580-6.
31. Dell'Italia LJ, Walsh RA. Application of a time varying elastance model to right ventricular performance in man. *Cardiovasc Res*. 1988;22:864-74.

Clin Orthop Relat Res (2009) 467:3149–3155
DOI 10.1007/s11999-009-0899-2

Synthetic Alginate is a Carrier of OP-1 for Bone Induction

Katsuhiko Nanno MD, Kenjiro Sugiyasu MD, Takashi Daimon PhD, Hideki Yoshikawa MD, PhD, Akira Myoui MD, PhD

Published online: 28 May 2009

Abstract Bone morphogenetic proteins (BMPs) can induce bone formation in vivo when combined with appropriate carriers. Several materials, including animal collagens and synthetic polymers, have been evaluated as carriers for BMPs. We examined alginate, an approved biomaterial for human use, as a carrier for BMP-7. In a mouse model of ectopic bone formation, the following four carriers for recombinant human OP-1 (BMP-7) were tested: alginate crosslinked by divalent cations (DC alginate), alginate crosslinked by covalent bonds (CB alginate), Type I atelocollagen, and poly-D,L-lactic acid-polyethyleneglycol block copolymer (PLA-PEG). Discs of carrier materials (5-mm diameter) containing OP-1 (3–30 μg) were implanted beneath the fascia of the back muscles in six mice per group. These discs were recovered 3 weeks after implantation and subjected to radiographic and histologic studies. Ectopic bone formation occurred in a dose-dependent manner after the implantation of DC alginate, atelocollagen, and PLA-PEG, but occurred only at the highest dose implanted with CB alginate. Bone formation with DC alginate/OP-1 composites was equivalent to that with atelocollagen/OP-1 composites. Our data suggest DC alginate, a material free of animal products that is already approved by the FDA and other authorities, is a safe and potent carrier for OP-1. This carrier may also be applicable to various other situations in the orthopaedic field.

One or more of the authors have received funding from Stryker Biotech K. K. (Tokyo, Japan) (AM) and from the Japan Science and Technology Agency (AM).
Each author certifies that his or her institution has approved the animal protocol for this investigation and that all investigations were conducted in conformity with ethical principles of research.
This work was performed at Department of Orthopaedic Surgery, Osaka University Graduate School of Medicine, Osaka, Japan.

K. Nanno, K. Sugiyasu, H. Yoshikawa (✉), A. Myoui
Department of Orthopaedic Surgery, Osaka University Graduate School of Medicine, 2-2 Yamadaoka, Suita, Osaka 565-0871, Japan
e-mail: yhideki@ort.med.osaka-u.ac.jp

T. Daimon, A. Myoui
Medical Center for Translational Research, Osaka University Hospital, 2-15 Yamadaoka, Suita, Osaka, Japan

Introduction

The repair capacity of human bone appears to depend on different very complex processes, such as vascularization, biomechanics, and topography. When damage is severe, as occurs with comminuted fractures or large bone defects after tumor resection, it is difficult for bone union to be achieved [6]. In such cases, autologous or allogenic bone grafting has been used. Autologous bone grafting is common and is still the gold standard, but has several disadvantages, including a limited supply of suitable bone and the risk of chronic pain, nerve damage, fracture, and cosmetic problems at the donor site. Allografts have no donor site problems, but there is the potential risk of disease or an immunologic reaction [10, 21]. For these reasons, the use of bone substitutes such as calcium phosphate-based porous ceramics has been increasing [18, 33]. These bioceramics are highly biocompatible and demonstrate osteoconduction, which is the ability to bind to bone matrix directly. However, they have no osteoinduction, which is the ability to induce new bone formation at ectopic sites.

Bone morphogenetic proteins (BMPs) belong to the transforming growth factor superfamily, are known to elicit new bone formation in vivo, and may play a leading role in

bone tissue engineering [36, 38]. To date, three types of BMP-based bone tissue engineering have been tried, which are cell therapy, gene therapy, and cytokine therapy [27]. Cell therapy involves the transplantation of autologous bone marrow mesenchymal cells after differentiation has been induced by BMP, but considerable resources and time are needed to culture the necessary cells [22, 34]. Gene therapy involves the transduction of genes encoding BMPs into cells at the site of damage [2, 7]. BMP-transduced cells may work more efficiently, compared with a single dose of recombinant cytokine therapy. However, gene therapy still has unsolved problems such as tumorigenesis and immunogenicity. Cytokine therapy involves the implantation of BMPs together with a carrier material that acts as a drug delivery system. We believe cytokine therapy is the most promising of these three approaches in terms of practical application. Cytokine therapy seems most convenient and safe, but the cost is very high because a large amount of BMP is required to achieve bone growth in humans. To increase the cost effectiveness of BMP, an appropriate carrier material is necessary.

Previous studies have indicated adequate in vivo new bone formation cannot be obtained by simply injecting a solution of BMP into the area where bone is needed [32]. For cytokine therapy, an appropriate carrier material is needed that retains BMP and releases it slowly, while serving as a scaffold for new bone formation [28, 29]. Several materials have already been evaluated as BMP carriers, including collagen obtained from animal sources [3, 11, 13, 31], synthetic polymers [14, 15, 19], tricalcium phosphate [17], and other inorganic materials [16]. Atelocollagen is a well-established BMP carrier, and has already been used clinically. PLA-PEG [20], one of the synthetic polymers, has been reported as a potent carrier for BMPs [23, 25, 26]. Although all of these materials can induce bone formation at ectopic and orthotopic sites, none of them has achieved widespread use because of disadvantages, such as the potential risk of disease transmission, fragility, stickiness, and difficulty in obtaining approval for clinical use [1, 4, 5, 14]. We therefore focused on alginate, which is already approved by the FDA for human use as a wound dressing and food additive [8, 37].

Alginate is a water-soluble linear polysaccharide extracted from brown seaweed that is composed of one to four linked α-L-gluronic and β-D-mannuronic acid monomers [9]. Gelation of alginate occurs as a result of crosslinking by divalent cations or covalent bonds [30]. Therefore, two types of alginate wound dressing products are available on the market and both effectively promote wound healing by maintaining a moist environment. One is an alginate crosslinked by divalent cations (DC alginate) and the other is an alginate crosslinked by covalent bonds (CB alginate).

To determine whether alginate can be a carrier for BMP, we compared four materials as carriers for OP-1(BMP-7) using the bone mineral content (BMC) measurement and alkaline phosphatase (ALP) activity measurement of the bone nodules ectopically induced by carrier materials/OP-1 composites. The four materials were DC alginate, CB alginate, atelocollagen, and PLA-PEG. We hypothesized: (1) BMC of bone nodules ectopically induced by DC alginate/OP-1 composite and/or CB alginate/OP-1 composite are equivalent or superior to those by atelocollagen and PLA-PEG; (2) ALP activity of bone nodules ectopically induced by DC alginate/OP-1 composite and/or CB alginate/OP-1 composite are equivalent or superior to those by atelocollagen and PLA-PEG by radiographic appearance and histology of the ectopic bone nodules; and (3) DC alginate and/or CB alginate have appropriate in vitro release kinetics of OP-1 equivalent to atelocollagen and PLA-PEG.

Materials and Methods

To verify our first hypothesis, we designed the following experiment (Experiment 1; Table 1). For each dose of OP-1 (3, 10, and 30 μg), 24 4-week-old male ICR mice were assigned to four equally sized independent groups after they were housed and acclimatized in cages with free access to food and water for 1 week. The four independent groups were DC alginate group, CB alginate group, atelocollagen group, and PLA-PEG group. The mice were anesthetized by intraperitoneal injection of pentobarbital. As reported previously [14, 15], carrier material/OP-1 composites were implanted beneath the fascia of the back muscles on the left side (one composite per animal). The experiment was designed under the assumption that the justifiable difference (effect size) between the atelocollagen group as a control and the other groups was 6 mg in BMC and the standard deviation within each group was 3 from the result of the previous study [24]. For the experiment to detect the difference at the 5% significance level with 90% power in the one-way analysis of variance, the necessary number of mice per group was six. Three weeks after implantation, these mice were killed and ectopic bone induced at the implantation site was harvested for further evaluation, including BMC measurement, radiography, and histological examination. The experimental protocol was approved by the Animal Experiment Committee of Osaka University, and the experiments were carried out in accordance with the Osaka University guidelines for care and use of laboratory animals.

To verify the second hypothesis, we repeated the Experiment 1 and obtained radiographs and measured ALP activity (Experiment 2; Table 1).

Table 1. Study groups and experimental design

Experiments	Carrier materials	Dose of OP-1	n	Examination
Experiment 1	DC alginate	3, 10, and 30 μg	18*	BMC, radiography, histology
	CB alginate	3, 10, and 30 μg	18*	BMC, radiography, histology
	Atelocollagen	3, 10, and 30 μg	18*	BMC, radiography, histology
	PLA-PEG	3, 10, and 30 μg	18*	BMC, radiography, histology
Experiment 2	DC alginate	3, 10, and 30 μg	18*	Radiography, ALP activity
	CB alginate	3, 10, and 30 μg	18*	Radiography, ALP activity
	Atelocollagen	3, 10, and 30 μg	18*	Radiography, ALP activity
	PLA-PEG	3, 10, and 30 μg	18*	Radiography, ALP activity

*: n = 6, each dose.

The BMC of the harvested discs was determined by dual-energy xray absorptiometry (DXA) using an animal bone densitometer (PIXImus; Lunar Corp, Madison, WI) and was expressed as milligrams per ossicle. Radiographs were obtained with a soft xray apparatus (MX-20 Faxitron®; Torrex and Micro Focus Systems, Wheeling, IL).

To measure ALP activity, the harvested discs were crushed, homogenized in 0.2% Nonidet® P-40 containing 1 mmol/L $MgCl_2$, and centrifuged at 10,000 rpm for 1 minute at 4°C. The supernatants thus obtained were assayed for ALP activity with an Alkaline Phospha B-Test Wako kit (Wako Pure Chemical Industries, Ltd, Osaka, Japan) using p-nitrophenyl phosphate (p-NP) as a substrate. The protein content was measured with a Pierce® BCA protein assay kit (Thermo Fisher Scientific Inc, Rockford, IL), and ALP activity was standardized by the protein content and expressed as nmol p-NP/minute/mg protein.

After radiography and BMC measurement, the samples were fixed in 10% neutral formalin, decalcified with ethylenediaminetetraacetic acid (pH 7.4), dehydrated in a graded ethanol series, and embedded in paraffin. One section per group with the largest tissue area (5-μm thick) were cut and stained with hematoxylin and eosin for observation under a light microscope. The formation of new bone, new bone marrow, degradation of the materials, and inflammatory change were evaluated by a pathologist (AM) and an orthopaedic surgeon (KN).

To verify the third hypothesis that DC alginate and/or CB alginate have appropriate in vitro release kinetics of OP-1, we incubated carrier materials/OP-1 composites in centrifuge tubes containing 1000 μL phosphate-buffered saline (PBS; Invitrogen, Carlsbad, CA) and kept for 21 days at 37°C. For each composite group, three samples were examined. The PBS in the tubes was replaced every 2 days, and then 100 μL was collected for assay after 24 hours. The amount of OP-1 was determined by measurement with a commercial BMP-7 ELISA kit (R&D Systems Inc, Minneapolis, MN) on days 1, 3, 7, 13, and 21 according to the manufacturer's instruction.

OP-1 (BMP-7 in a lyophilized 5% lactose formulation) was provided by Stryker Biotech (Hopkinton, MA). OP-1 was dissolved in distilled water at a concentration of 2 μg/μL. DC alginate (ARGODERM®; crosslinked by Ca^{2+}), CB alginate (KURABIO®), and atelocollagen (INSTAT®) were purchased from Smith & Nephew (London, UK), Koyo Sangyo Co, Ltd (Tokyo, Japan), and Johnson & Johnson (New Brunswick, NJ), respectively. PLA-PEG with a total molecular weight of 11,400 Da and a PLA:PEG molar ratio of 51:49 was synthesized and provided by Taki Chemicals Co, Ltd (Hyogo, Japan).

To prepare carrier material/OP-1 composites, sheets of DC alginate, CB alginate, and atelocollagen were cut into discs (5-mm diameter). Then 25 μL of a solution containing 3, 10, or 30 μg OP-1 was added dropwise to each disc, after which the discs were freeze-dried and stored at −20°C until implantation into mice. All procedures were carried out under sterile conditions.

PLA-PEG/OP-1 composites were prepared as described previously [25]. Briefly, 10 mg of the polymer was liquefied in 50 μL acetone and mixed with 3, 10, or 30 μg OP-1. Each mixture was evaporated to dryness to remove acetone in a safety cabinet, fabricated into a disc-shaped implant, and stored at −20°C until implantation into mice.

To verify the first and second hypotheses, we used one-way analysis of variance (ANOVA), followed by a post hoc Scheffe's test. For each of these statistical analyses, the data sets met the assumptions of normality ($p > 0.15$ by the Jarque-Bera test [12]) justifying the use of parametric models. All analyses were performed using the R software program (Version 2.8.1;R Foundation for Statistical Computing).

Results

With 3 μg OP-1, BMC of the new bone in the DC alginate group was greater than that in atelocollagen group ($p = 0.0234$) and PLA-PEG group ($p = 0.0009$). With

30 μg OP-1, however, we observed no differences among the DC alginate, atelocollagen, and PLA-PEG. On the other hand, BMC of CB alginate group was very low compared with the other groups (Fig. 1). The results suggest that the BMC of DC alginate group was superior to those of atelocollagen and PLA-PEG groups, especially with a low dose of OP-1.

In the DC alginate group, ALP activity was high independent of the OP-1 dose. With 3 μg OP-1, DC alginate/OP-1 composites exhibited higher ALP activity than atelocollagen group ($p = 0.0071$) and PLA-PEG group ($p = 0.0001$) (by Scheffe's test). ALP activity of the CB alginate group was very low compared with the other groups (Fig. 2). The results suggest that ALP activity of the DC alginate group was superior to those of atelocollagen and PLA-PEG groups, especially with a low dose of OP-1.

In the release study of OP-1, the maximum concentration of OP-1 in the supernatant was detected on Day 1, followed by a steady decline. The decline of OP-1 levels in the atelocollagen group was faster than that in the other groups. In the DC alginate group, the decrease of OP-1 levels was the slowest and the concentration of OP-1 was still higher than 200 ng/mL on Day 21 (Fig. 3). These data suggested that DC alginate retains OP-1 and releases it most slowly compared to atelocollagen and PLA-PEG.

In the additionally performed radiographic examination of the bone nodules, obvious bone formation was only detected in the DC alginate and atelocollagen groups with 3 μg OP-1 (Fig. 4A–D). In the CB alginate group, new bone formation was observed only with 30 μg OP-1. The results of the additionally performed histological examination were consistent with the radiographic findings. In the DC alginate and atelocollagen groups, abundant new bone formation that contained normal hematopoietic bone marrow was observed even at low dose of OP-1. In the CB alginate group, however, new bone formation was very poor at low dose of OP-1. With 30 μg OP-1, irrespective of the carrier materials, newly formed bone had a thin cortex

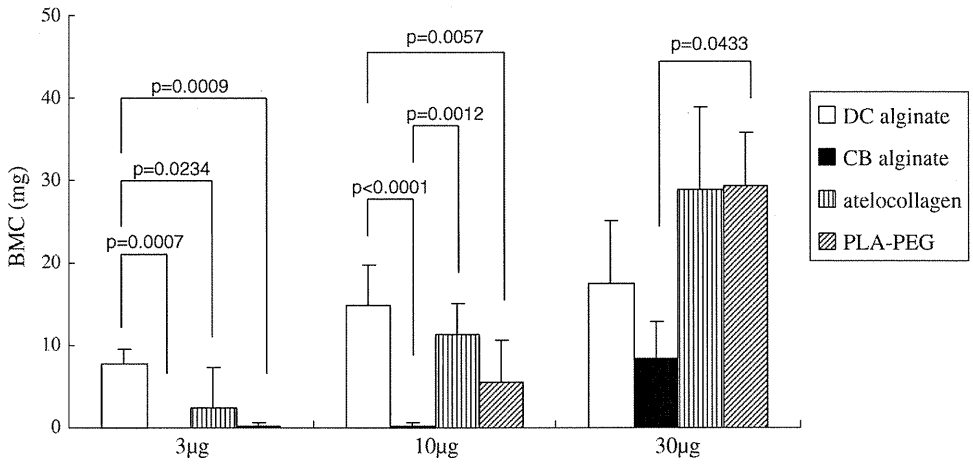

Fig. 1 In each carrier material group, BMC was measured by DXA using a PIXImus animal densitometer. BMC increased in an OP-1-dose dependent manner with every carrier material. With 3 μg and 10 μg OP-1, the BMC of the new bone in the DC alginate group was greater than that in the other groups.

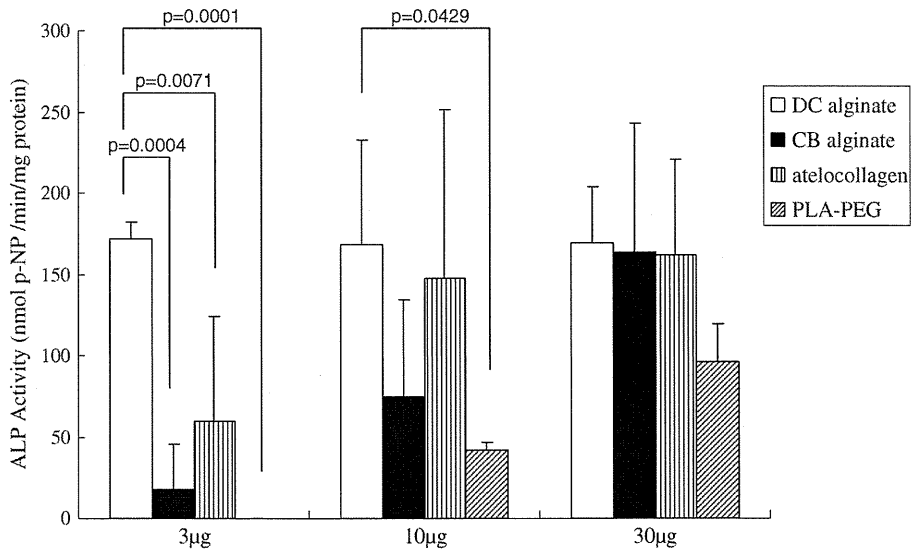

Fig. 2 ALP activity of ectopic bone was measured by using p-NP as a substrate. In the CB alginate, atelocollagen, and PLA-PEG groups, ALP activity increased in a dose-dependent manner. In the DC alginate group, ALP activity was relatively high independent of the dose of OP-1.

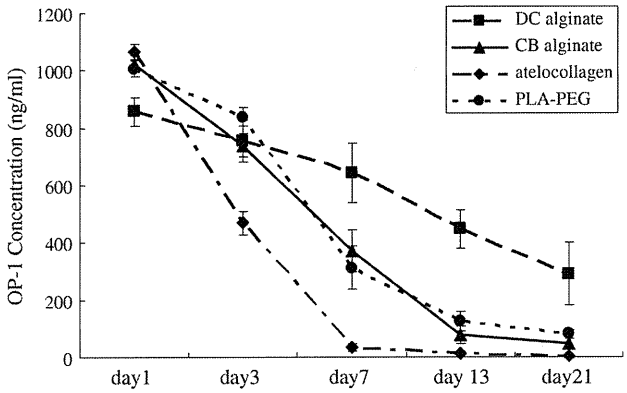

Fig. 3 OP-1 release from each carrier material/OP-1 (30 μg) composite was measured over time by a commercial BMP-7 ELISA kit. With each carrier material, the maximum concentration of OP-1 was detected on Day 1 and it decreased afterward. The decline was slowest in the DC alginate group.

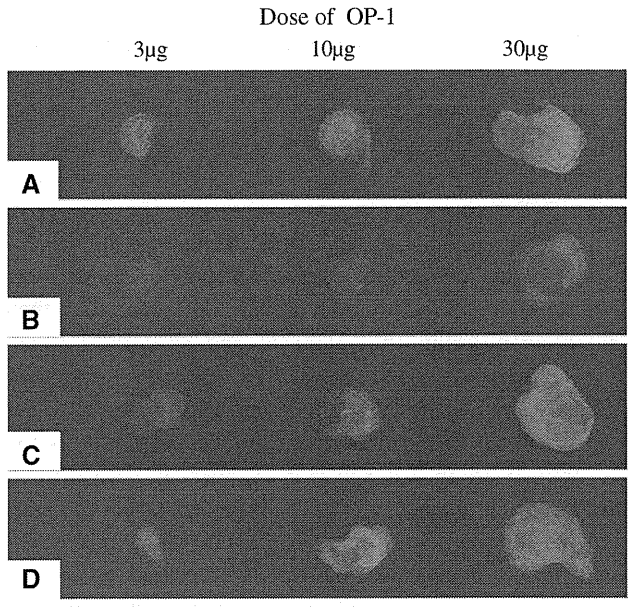

Fig. 4A–D The carriers for OP-1 tested were (**A**) DC alginate, (**B**) CB alginate, (**C**) atelocollagen, and (**D**) PLA-PEG. Soft xray photographs of ectopic bone induced by OP-1 (3, 10, or 30 μg) show bone formation with the DC alginate/OP-1 composite is equivalent or superior to that induced by the other carrier/OP-1 composites.

surrounding cancellous bone that contained hematopoietic bone marrow, and no inflammatory change was observed (Fig. 5A–D). These additional results were compatible with the results of BMC and ALP activity, suggesting that DC alginate can be an equivalent or superior carrier for a low dose of OP-1 compared with atelocollagen and PLA-PEG.

Discussion

Various materials have already been evaluated as carriers for BMPs, but they all have some disadvantages as mentioned previously. This study was designed to examine whether alginate, a material with no animal product content, is an equivalent or superior carrier for OP-1(BMP-7) compared with atelocollagen and PLA-PEG. Specifically we hypothesized: (1) BMC of bone nodules ectopically induced by DC alginate/OP-1 composite and/or CB alginate/OP-1 composite are equivalent or superior to those by atelocollagen and PLA-PEG; (2) ALP activity of bone nodules ectopically induced by DC alginate/OP-1 composite and/or CB alginate/OP-1 composite are equivalent or superior to those by atelocollagen and PLA-PEG; and (3) DC alginate and/or CB alginate have appropriate in vitro release kinetics of OP-1 equivalent to atelocollagen and PLA-PEG.

This study has several limitations. First, DC alginate was originally approved for clinical use as a cutaneous wound dressing [8, 37]. Therefore, its biodegradability and immunogenicity are unclear during use at a deeper site. Second, in the histological examination, DC alginate remained at the center of the new ectopic bone, indicating it had not degraded within 3 weeks. Although no inflammatory reaction was found, longer observation will be necessary before this material can be used with confidence at deeper sites. Third, ALP activity is a marker for osteoblastic differentiation, and is high in the early stage of osteoblast lineage. ALP activity is not necessarily parallel to the activity of bone formation. Fourth, in the release study, a commercial BMP-7 ELISA kit can only detect the amount of BMP-7(OP-1) protein, but cannot evaluate the activity of OP-1. The result of a release test may not reflect the actual activity of OP-1 released from carriers in vivo.

To determine whether DC alginate and/or CB alginate are equivalent or superior carriers for OP-1 compared with atelocollagen and PLA-PEG, we measured BMC of ectopic bone nodules as a primary research question. A previous study [24] reported that BMC of the ectopic bone induced by PLA-PEG/BMP-2 composite is about 6 mg higher than that by atelocollagen/BMP-2 composite. In our study, the BMC of DC alginate/OP-1 (3 μg) composite was about 6 mg higher than that of the atelocollagen/OP-1 (3 μg) composite and even much higher than that of CB alginate and PLA-PEG. The result of BMC measurement suggested that DC alginate is a highly effective carrier that enhances the bone-inducing effect of OP-1 even when OP-1 content is low.

The result of ALP activity measurement was compatible with the result of BMC, which reinforced the hypothesis that DC alginate is an equivalent or superior carrier compared with the other materials. Upon histological examination, not only trabecular bone but also normal hematopoietic bone marrow was observed, and we found

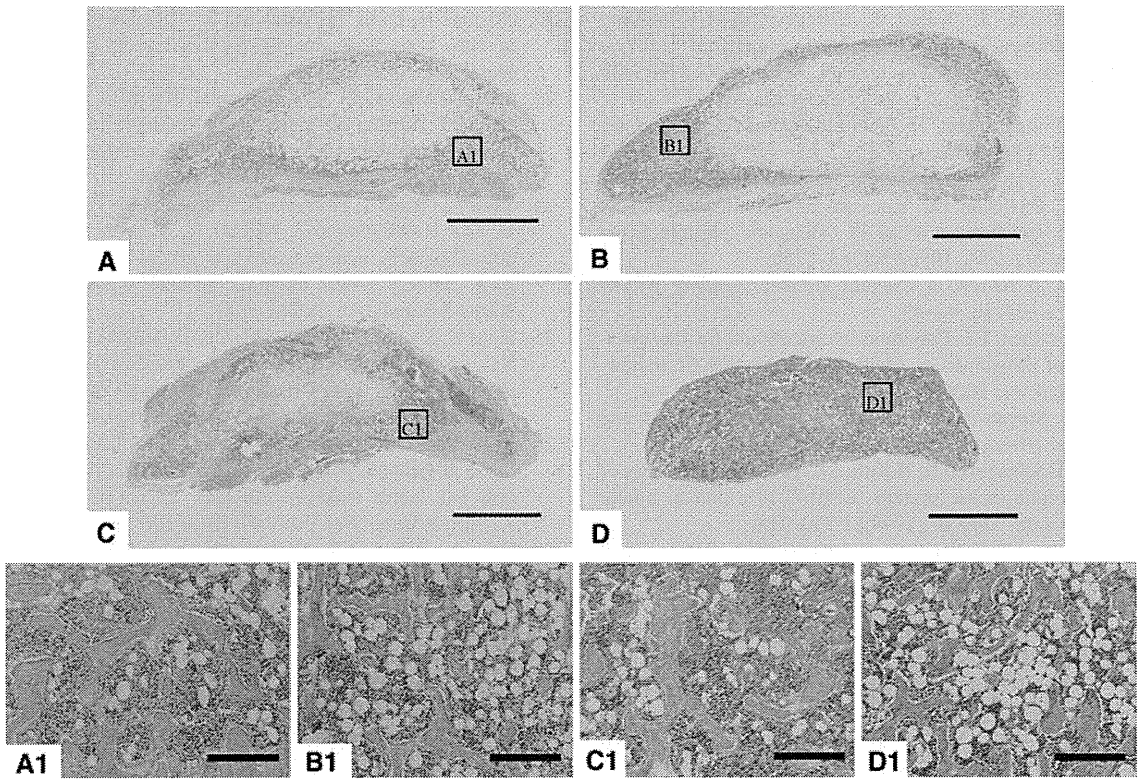

Fig. 5A–D Representative photomicrographs of the ectopic bone formation induced by OP-1 (30 μg) are shown (**A**, A1: DC alginate; **B**, B1: CB alginate; **C**, C1: atelocollagen; **D**, D1: PLA-PEG) (**A–D**: stain, hematoxylin and eosin; original magnification, ×10; scale bar = 2 mm; A1–D1: stain, hematoxylin and eosin; original magnification, ×100; scale bar = 200 μm). Irrespective of the carrier material, the newly formed bone had a thin cortex surrounding cancellous bone that contained highly cellular bone marrow.

no accumulation of inflammatory cells, such as monocyte/macrophages. The histological appearance of the ectopic bone induced by DC alginate/OP-1 composite seemed similar to that by atelocollagen/OP-1 composite, which is considered a safe biomaterial in terms of immunological response. These data suggested that DC alginate appears likely a safe material with no inflammatory response even when used in a deep site.

In contrast, CB alginate achieved relatively poor bone formation, especially with a low dose of OP-1. DC alginate and CB alginate only differ in the mode of crosslinking, but the release of OP-1 from these two alginates was quite different. It is known crosslinking by divalent cations forms a characteristic egg box structure that is suitable for trapping proteins in alginate [9]. Thus, the difference of bone formation between these two types of alginate may be partly due to a difference in their ability to retain OP-1 and release it slowly. It is also known the number of carboxyl residues in DC alginate is larger than that in CB alginate. The carboxyl residues induce apatite nucleation followed by the deposition of hydroxyapatite crystals on the alginate [35]. Furthermore, the Ca^{2+} contained in DC alginate can be utilized for new calcified bone, which is an advantage compared with CB alginate.

In conclusion, our data suggest DC alginate, a material with no animal product content that is approved by the FDA and other authorities, is a safe and potent carrier for OP-1. It is of note that DC alginate strongly potentiates osteoinduction of OP-1 even at a low dose. Thus, its use may reduce the cost of OP-1-based bone regeneration therapy.

Acknowledgments We thank Stryker Biotech, Smith & Nephew, Koyo Sangyo Co, Ltd, Johnson & Johnson, and Taki Chemicals Co, Ltd, for kindly providing the chemicals and materials.

References

1. Bach FH, Fishman JA, Daniels N, Proimos J, Anderson B, Carpenter CB, Forrow L, Robson SC, Fineberg HV. Uncertainty in xenotransplantation: individual benefit versus collective risk. *Nature Med.* 1998;4:141–144.
2. Bonadio J, Smiley E, Patil P, Goldstein S. Localized, direct plasmid gene delivery in vivo: prolonged therapy results in reproducible tissue regeneration. *Nature Med.* 1999;5:753–759.
3. Burkus JK, Dorchak JD, Sanders DL. Radiographic assessment of interbody fusion using recombinant human bone morphogenetic protein type 2. *Spine.* 2003;28:372–377.
4. Butler D, Wadman M, Lehrman S, Schiermeier Q. Last chance to stop and think on risks of xenotransplants. *Nature.* 1998;391: 320–324.